Differentiating dark interactions with perturbation

Srijita Sinha*

Indian Institute of Science Education and Research Kolkata, Mohanpur, Nadia, 741246, India

(Received 22 January 2021; accepted 3 June 2021; published 28 June 2021)

A cosmological model with an energy transfer between dark matter (DM) and dark energy (DE) can give rise to comparable energy densities at the present epoch. The present work deals with the perturbation analysis, parameter estimation, and Bayesian evidence calculation of interacting models with dynamical coupling parameter that determines the strength of the interaction. We have considered two cases, where the interaction is a more recent phenomenon and where the interaction is a phenomenon in the distant past. Moreover, we have considered the quintessence DE equation of state with Chevallier-Polarski-Linder (CPL) parametrization and energy flow from DM to DE. Using the current observational datasets like the cosmic microwave background (CMB), baryon acoustic oscillation (BAO), Type Ia Supernovae (SNe Ia), and redshift-space distortions (RSD), we have estimated the mean values of the parameters. Using the perturbation analysis and Bayesian evidence calculation, we have shown that interaction present as a brief early phenomenon is preferred over a recent interaction.

DOI: 10.1103/PhysRevD.103.123547

I. INTRODUCTION

The discovery that the Universe is expanding with an acceleration [1–4] has set a new milestone in the history of cosmology. This discovery also presented a new challenge as explaining this phenomenon requires an agent that leads to a repulsive gravity. The flurry of more recent high precision observational data [5–13] has consolidated the fact that the Universe indeed gravitates in the wrong way. Many theoretical models have been put forward to explain the repulsive nature of gravity, but arguably the most popularly accepted one is the presence of an exotic component named "dark energy." This exotic component of the contents of the Universe can produce a sufficient negative pressure, which overcomes the gravitational attraction of matter and drives the recent acceleration. The cosmological constant, Λ [6,14–19] is the first preferred choice, followed by a scalar field with a potential [20–28]. The other popular choices include holographic dark energy [29–36], Chaplygin gas [37–42], phantom field [43,44], quintom model [45,46], to name a few. The list of candidates as dark energy is far from being complete in the absence of a universally accepted one. There are excellent reviews [47–50] on these candidates.

The observationally most preferred model, Λ with cold dark matter (ΛCDM), faces many problems like the so-called "cosmological constant problem" [23,51] and the coincidence problem [52,53]. The cosmological constant problem is the discrepancy between the theoretical value and the observed value of the cosmological constant. The coincidence problem is the question, why both dark matter and dark energy have comparable energy densities precisely at the present epoch? These problems in the simple ΛCDM model are the motivation to search for other possible avenues.

The fact that dark matter and dark energy have energy densities of the same order of magnitude opens the possibility that there is an energy exchange between the two. Interactions between dark matter and dark energy in various dark energy models have been studied and tested against observations extensively [54–80]. For detailed reviews on interacting dark matter-dark energy models, we refer to [81–83].

The presence of a coupling in the dark sector may not be ruled out *a priori* [54–77,84–88]. It naturally raises the question whether the interaction was there from the beginning of the Universe and exists through its evolution or is a recent phenomenon, or it was entirely an early phenomenon and not at all present today. A modification of the phenomenological interaction term by an evolving coupling parameter instead of its being a constant, may answer this question. A constant coupling parameter indicates the interaction is present throughout the evolution of the Universe [59,89]. In this work, we have considered the coupling parameter to be evolving with the scale factor. Interaction with an evolving coupling parameter is not studied much in literature and warrants a detailed analysis. Rosenfeld [90] and Yang *et al.* [91] have considered the dynamical coupling parameter, but the motivation as well as the analytical form of the parameter used in the present work are different.

There is no theoretically preferred form of the phenomenological interaction term. In this work, two possible

*ss13ip012@iiserkol.ac.in

scenarios are considered—(a) the presence of interaction is significant during the late time but not at early time and (b) the presence of interaction is significant in the early times but not at late time. The rate of energy transfer is considered to be proportional to the dark energy density. The dynamical coupling parameter will affect the evolution of the dark matter and hence have its imprints in the growth of perturbations. Thus the presence of dynamical interaction can give rise to new features in structure formation. The motivation of the present work is to investigate the effect of interactions on clustering of matter perturbation and test the models against observational datasets.

We have tested the interacting models with different observational datasets like the cosmic microwave background (CMB) [6], baryon acoustic oscillation (BAO) [9,92,93], type Ia supernovae (SNe Ia) [4] data and their different combinations. For a complete understanding of the effect of interaction on structure formation, it is necessary to consider the effect of the large scale structure (LSS) information on the cosmological constraints. In the present work, we have considered the redshift-space distortions (RSD) data [94] as the LSS data. Combining the RSD data with CMB, BAO and Supernovae data is expected to break the degeneracy between the different interacting models with similar background evolution as well as provide a tight constraint on the interaction parameter.

The LSS data, which includes Planck Sunyaev-Zel'dovich survey [95], Canada France Hawaii Telescope Lensing Survey (CFHTLens) [96,97], South Pole Telescope (SPT) [98,99], RSD survey, are in disagreement with CMB observations for the root-mean-square mass fluctuation in spheres with radius $8h^{-1}$ Mpc, (called σ_8) and hence for the matter density parameter Ω_m and the Hubble parameter H_0 [19,100–106]. The LSS observations prefer lower values of σ_8 and Ω_m and a higher value of H_0 compared to the CMB results. Many attempts have been made to settle the disagreement between the two datasets [107–112]. Some more of the notable work with RSD data are [36,70,113–119].

The most persisting tension in observational cosmology is the discrepancy in the value of the Hubble parameter, H_0, as provided by the CMB measurement from the *Planck* satellite and the local measurements like the supernovae and H_0 for the equation of state (SH0ES) project [120–122]. The distance-ladder estimate of $H_0 = 74.03 \pm 1.42$ km s^{-1} Mpc^{-1} from the latest Hubble Space Telescope (HST) data [122] increases the tension with the recent CMB measurement of $H_0 = 67.36 \pm 0.54$ km s^{-1} Mpc^{-1} [6] to 4.4σ. Other distance-ladder probes like the LIGO [123], H0LiCOW [124] do not seem to relieve the tension. The H_0 tension is more severe than the σ_8 tension. The σ_8 and H_0 tensions can be attributed to the possible systematics in the CMB or local measurements [125–128]. On the other hand, these tensions strengthen the reason to search for models other than the simple ΛCDM model. In spite of the many attempts [129–137] toward the resolution, the tension still persists. For detail review on H_0 tension, we refer to [138,139]. A nongravitational interaction between the dark components is often introduced to attempt a resolution to the tension with some success. The simplest interacting model without introducing any new degrees of freedom is the interaction of dark matter with the inhomogeneous vacuum energy density as shown in [17,19,42,69,119,140–146]. Many other interacting dark energy models have been studied thoroughly in the literature [70,78,135,136,146–154].

It must be mentioned here that the model with constant coupling parameter has been tested rigorously against different observational datasets and priors ranges [19,146,151] to name a few. In this work, we used different datasets and different prior ranges and an "evolving" coupling parameter in the interaction term. Moreover, we considered an evolving dark energy with EoS given by the Chevallier-Polarski-Linder (CPL) parametrization. However, the present work is not an attempt to alleviate the σ_8 or H_0 tensions but to understand the evolution of the interaction using perturbation and test the models against observational datasets.

The paper is organized as follows. Section II discusses the background equations of interacting dark matter-dark energy models. The perturbation equations, evolution of the density contrast along with the effects on the cosmic microwave background (CMB) temperature fluctuation, matter power spectrum, linear growth rate and $f\sigma_8$ are discussed in Sec. III. In Sec. IV, we discuss the results obtained from constraining the interacting models against different observational datasets performing the Markov Chain Monte Carlo (MCMC) analysis and in Sec. V, we discuss our inference from Bayesian evidence calculation. Finally, in Sec. VI, we conclude with a summary and a brief discussion of the results that we arrived at. The details on the datasets used and the method are given in Appendixes A and B.

II. INTERACTING DARK MATTER-DARK ENERGY FLUID

The Universe is considered to be described by a spatially flat, homogeneous and isotropic Friedmann-Lemaître-Robertson-Walker (FLRW) metric,

$$ds^2 = a^2(\tau)(-d\tau^2 + \delta_{ij}dx^i dx^j), \tag{1}$$

where $a(\tau)$ is the conformal scale factor and the relation between conformal time (τ) and cosmic time (t) is $a^2 d\tau^2 = dt^2$. Using the metric [Eq. (1)], the Friedmann equations are written as

$$3\mathcal{H}^2 = -a^2\kappa\sum_A \rho_A, \tag{2}$$

$$\mathcal{H}^2 + 2\mathcal{H}' = a^2\kappa\sum_A p_A, \tag{3}$$

where $\kappa = 8\pi G_N$ (G_N being the Newtonian gravitational constant), $\mathcal{H}(\tau) = \frac{a'}{a}$ is the Hubble parameter, and ρ_A and p_A are respectively the energy density and pressure of the different components of the Universe. A prime indicates differentiation with respect to the conformal time τ. The Universe is filled with five components of matter, all formally represented as perfect fluids—photons (γ), neutrinos (ν), baryons (b), cold dark matter (c) and dark energy (de). We assume that there is an energy transfer only in the dark sector of the Universe such that the conservation equations are

$$\rho_c' + 3\mathcal{H}\rho_c = -aQ, \tag{4}$$

$$\rho_{\rm de}' + 3\mathcal{H}(1 + w_{\rm de})\rho_{\rm de} = aQ. \tag{5}$$

The pressure, $p_c = 0$ for cold dark matter. The other three fluids—photons (γ), neutrinos (ν) and baryons (b) conserve independently and hence, have no energy transfer among them. Their conservation equations are written as

$$\rho_A' + 3\mathcal{H}(1 + w_A)\rho_A = 0, \tag{6}$$

where $w_A = p_A/\rho_A$ is the equation of state parameter (EoS) of the Ath fluid and $A = \gamma, \nu, b$. For photons and neutrinos, the EoS parameter is $w_\gamma = w_\nu = 1/3$, for baryons and cold dark matter, the EoS parameter is $w_b = w_c = 0$ and for dark energy, the EoS parameter is $w_{\rm de} = p_{\rm de}/\rho_{\rm de}$.

In Eqs. (4) and (5), Q gives the rate of energy transfer between the two fluids. If $Q < 0$, energy is transferred from dark energy to dark matter (DE → DM) and if $Q > 0$, energy is transferred from dark matter to dark energy (DM → DE). When $Q > 0$, dark matter redshifts faster than a^{-3} and when $Q < 0$, dark matter redshifts slower than a^{-3}. The dark energy evolution depends on the difference $w_{\rm de} - \frac{aQ}{3\mathcal{H}\rho_{\rm de}}$. Thus, the interaction manifests itself by changing the scale factor dependence of the dark matter as well as dark energy. There are different forms of the choice of the phenomenological interaction term Q, the models with Q proportional to either ρ_c or $\rho_{\rm de}$ or any combination of them are among the more popular choices, [61,70,77,155,156] to mention a few. It must be mentioned here that there is no particular theoretical compulsion for any of these choices. We have taken the covariant form of the source term such that it is proportional to the dark energy density ($Q^\mu \propto \rho_{\rm de}$) and is parallel to the matter 4-velocity ($Q^\mu \| u_c^\mu$) and is written as

$$Q^\mu = \frac{\mathcal{H}\rho_{\rm de}u_c^\mu\beta(a)}{a}. \tag{7}$$

Here, $\beta(a)$ is the coupling parameter evolving with the scale factor, a. The coupling parameter determines the strength of interaction and direction of energy flow; $\beta = 0$ indicates that there is no coupling in the dark sector. In this work, we considered two possible scenarios,

Model L: If the coupling was not significant in the early Universe ($a = 0$) and is felt only at the recent epoch.

Model E: If the interaction is predominantly an early phenomenon and is insignificant now ($a = 1$).

We compared the models with the Universe with a constant interaction parameter (*Model C*). The ansatz chosen for the models are simple analytic functions of a which are well-behaved in the region $a \in [0, 1]$.

$$\textbf{Model L}: \quad \beta(a) = \beta_0\left(\frac{2a}{1+a}\right), \tag{8a}$$

$$\textbf{Model E}: \quad \beta(a) = \beta_0\left(\frac{1-a}{1+a}\right), \tag{8b}$$

$$\textbf{Model C}: \quad \beta(a) = \beta_0. \tag{8c}$$

The terms in parenthesis in the Eqs. (8a) and (8b) are positive definite for the domain of a under consideration and hence the direction of energy flow is determined by the signature of the constant β_0.

It is considered in this work that the DE has a dynamical EoS parameter given by the well-known Chevallier-Polarski-Linder (CPL) parametrization [157,158] as

$$w_{\rm de} = w_0 + w_1(1 - a), \tag{9}$$

where w_0 and w_1 are constants. A dimensionless interaction term is defined as $\Omega_I = \frac{Q}{3H^3/\kappa}$ and the dimensionless density parameter of matter (baryonic matter and cold dark matter (DM), denoted as '$m(= b + c)$') and dark energy (DE) are defined as $\Omega_m = \frac{\rho_m}{3H^2/\kappa}$ and $\Omega_{\rm de} = \frac{\rho_{\rm de}}{3H^2/\kappa}$ respectively. Similarly, energy density parameter for radiation (denoted as "$r(= \gamma + \nu)$") is $\Omega_r = \frac{\rho_r}{3H^2/\kappa}$. Here H is the Hubble parameter defined with respect to the cosmic time t and the dimensionless Hubble parameter at the present epoch is defined as $h = \frac{H_0}{100\ {\rm km\,s^{-1}\,Mpc^{-1}}}$. The parameter values used in this work are listed in Table I, where the values are taken from the latest 2018 data release of the *Planck* collaboration [6] (*Planck* 2018, henceforth).

TABLE I. Values of parameters used in this work based on *Planck* 2018.

Parameter	Value
$\Omega_b h^2$	0.0223828
$\Omega_c h^2$	0.1201075
$H_0[{\rm km\,s^{-1}\,Mpc^{-1}}]$	67.32117

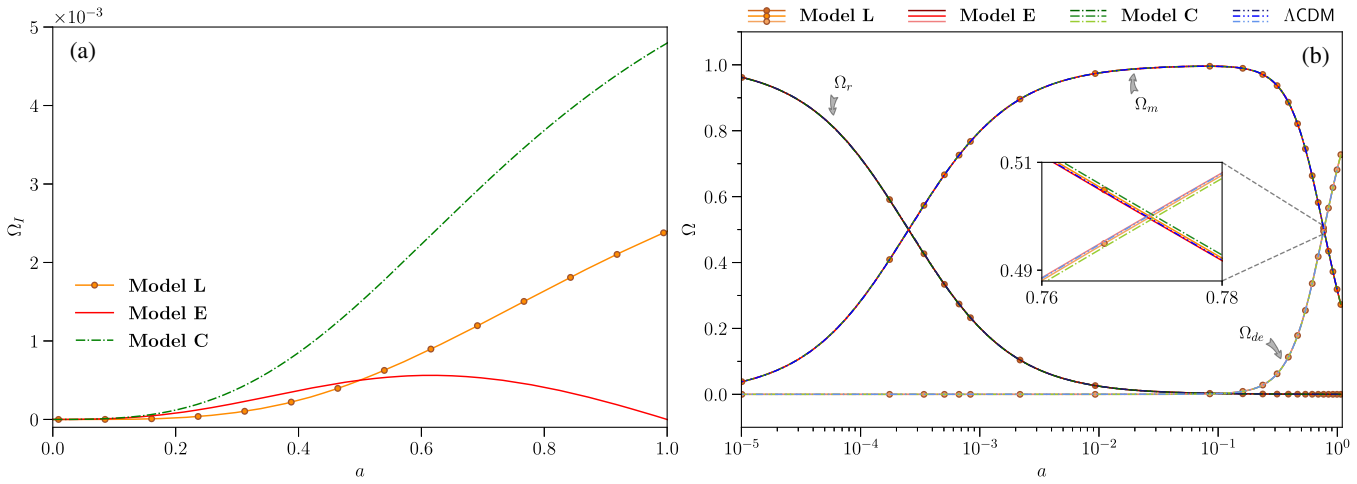

FIG. 1. Plot of (a) the dimensionless interaction parameter Ω_I and (b) density parameter Ω against scale factor a. The x-axis in Fig. (b) is in logarithmic scale The solid line with solid circles represents Model L, solid line represents Model E, and dashed-dot line represents Model C while the dashed-dot-dot line is for ΛCDM. The inset shows the zoomed-in portion for the region $a = 0.76$ to $a = 0.78$.

As shown by Pavón and Wang [159], energy transfer from dark energy to dark matter (DE → DM) is thermodynamically favored following the Le Châtelier-Braun principle. Observational data, on the other hand, prefer energy transfer from dark matter to dark energy (DM → DE) [34,77,78,87]. It must be noted that though the parameters β_0 and $w_{\rm de}$ are in principle independent, they largely affect the perturbation evolutions and hence are correlated in parameter space of perturbation constraints. It had been shown in [160–162] that gravitational instabilities arise for constant $w_{\rm de} \simeq -1$ due the interaction term in non-adiabatic pressure perturbations of dark energy. The early time instabilities in the evolution of dark energy perturbation [155,160,161,163–169] depend on the parameters β_0 and $(1 + w_{\rm de})$ via a ratio called the doom factor, given as

$$d \equiv -\frac{aQ}{3\mathcal{H}\rho_{\rm de}(1 + w_{\rm de})}. \tag{10}$$

To avoid early time instabilities, d must be negative semidefinite ($d \leq 0$) [163], ensuring that β_0 and $(1 + w_{\rm de})$ have the same sign. Thus stable perturbations can be achieved with either energy flow from dark matter to dark energy ($\beta_0 > 0$) and nonphantom or quintessence EoS ($(1 + w_{\rm de}) > 0$) or energy flow from dark energy to dark matter ($\beta_0 < 0$) and phantom EoS ($(1 + w_{\rm de}) < 0$).

In this section and the next (Sec. III), we have considered the energy flow from dark matter to dark energy and β_0 to be positive and hence $w_{\rm de} > -1$. We have chosen the magnitude of β_0 to be small consistent with the observational results given in [70,75,76,80,89]. The particular value used here, $\beta_0 = 0.007$, is an example chosen such that no instability in the dark energy perturbation arises. For the background and perturbation analyses (Sec. III), we have chosen the example values of the parameter, w_0 and w_1 in $w_{\rm de}$ [Eq. (9)] as

$$w_0 = -0.9995, \qquad w_1 = 0.005. \tag{11}$$

The chosen values of the parameters w_0 and w_1 also ensure that $w_{\rm de} \sim -1$ at $a = 1$. It must be mentioned that, EoS parameter in the quintessence region is considered solely to avoid DE models with a future "big-rip" singularity associated with phantom EoS parameter. Several instances of interacting DE models with $w_{\rm de} < -1$ are found in the literature [75–78,89,135,136,160,163]. Figure 1(a) shows the evolution of Ω_I with scale factor a for Model L, Model E and Model C. In Fig. 1(a) the direction of energy flow is from dark matter to dark energy and the magnitude of Ω_I is the rate of energy transfer. The variation of density parameters of radiation (Ω_r), dark matter together with baryons (Ω_m) and dark energy ($\Omega_{\rm de}$) with scale factor a in logarithmic scale is shown in Fig. 1(b) for the three models and the ΛCDM model. It is clear from Figs. 1(a) and 1(b) that the effect of interaction will be very small in its contribution to the density parameters, Ω_A, where $A = r, m, de$.

III. EVOLUTION OF PERTURBATIONS

The perturbed FLRW metric in a general gauge takes the form [170–172]

$$ds^2 = a^2(\tau)\{-(1 + 2\phi)d\tau^2 + 2\partial_i B d\tau dx^i + [(1 - 2\psi)\delta_{ij} + 2\partial_i\partial_j E]dx^i dx^j\}, \tag{12}$$

where ϕ, ψ, B, E are gauge-dependant scalar functions of space and time. In the presence of interaction, the covariant form of the energy-momentum conservation equation will be

$$T^{\mu\nu}_{(A);\nu} = Q^{\mu}_{(A)}, \quad \text{where} \sum_A Q^{\mu}_{(A)} = 0. \tag{13}$$

The energy-momentum transfer function for the fluid A, $Q^{\mu}_{(A)}$, can be split into the energy transfer rate, $Q_{(A)}$ and the momentum transfer rate, $F^{\mu}_{(A)}$, relative to the total 4-velocity as [155,160,162]

$$Q^{\mu}_{(A)} = Q_{(A)}u^{\mu} + F^{\mu}_{(A)}, \quad u_{\mu}F^{\mu}_{(A)} = 0, \quad F^{\mu}_{(A)} = a^{-1}(0, \partial^i f_A). \tag{14}$$

Writing the total 4-velocity, u^{μ}, in terms of the total peculiar velocity, v as

$$u^{\mu} = a^{-1}(1-\phi, v^i), \tag{15}$$

the temporal and spatial components of the 4-energy-momentum transfer rate can be written as

$$Q^{0}_{(A)} = a^{-1}[Q_A(1-\phi) + \delta Q_A], \tag{16}$$

$$\text{and} \quad Q^{i}_{(A)} = a^{-1}[Q_A v^i + \partial^i f_A] \tag{17}$$

respectively, where δQ_A is the perturbation in the energy transfer rate and f_A is the momentum transfer potential.

The perturbed conservation equations of the fluid A in the Fourier space are written as

$$\delta\rho_A' - 3(\rho_A + p_A)\psi' + k(\rho_A + p_A)(v_A + E') + 3\mathcal{H}(\delta\rho_A + \delta p_A) = aQ_A\phi + a\delta Q_A, \tag{18}$$

$$[(\rho_A + p_A)(v_A + B)]' + 4\mathcal{H}(\rho_A + p_A)(v_A + B) - k(\rho_A + p_A)\phi - k\delta p_A = aQ_A(v + B) - akf_A. \tag{19}$$

In Eqs. (18) and (19), $\delta\rho_A$ is the perturbation in the energy density, δp_A is the perturbation in pressure, $u^{\mu}_A = a^{-1}(1-\phi, v^i_A)$ is the 4-velocity with peculiar velocity v_A of the fluid A and k is the wave number. For an adiabatic perturbation, the pressure perturbation [160,173–176] in the presence of interaction is

$$\delta p_A = c^2_{s,A}\delta\rho_A + (c^2_{s,A} - c^2_{a,A})[3\mathcal{H}(1+w_A)\rho_A - aQ_A]\frac{v_A}{k}, \tag{20}$$

where $c^2_{a,A} = \frac{p_A'}{\rho_A'}$ is the square of adiabatic sound speed and $c^2_{s,A} = \frac{\delta p_A}{\delta\rho_A}$ is the square of effective sound speed in the rest frame of Ath fluid.

The dynamical coupling parameter β_0 defined in Eq. (7) in the previous section is considered to be not affected by perturbation. This assumption is valid for the EoS parameter defined in Eq. (9) and the Hubble parameter, $\mathcal{H}$. These perturbation equations are solved along with the perturbation equations [170–172] of the radiation, neutrino and baryon using the publicly available Boltzmann code CAMB[1] [177] after suitably modifying it.

Using (15), Eq. (7) can be conveniently written as

$$Q = \frac{\mathcal{H}\rho_{\rm de}\beta(a)}{a}. \tag{21}$$

Defining the density contrasts of the dark matter and dark energy as $\delta_c = \delta\rho_c/\rho_c$ and $\delta_{de} = \delta\rho_{de}/\rho_{de}$ respectively and using Eqs. (20) and (21), the perturbation Eqs. (18) and (19) are written in synchronous gauge [172] ($\phi = B = 0$, $\psi = \eta$ and $k^2E = -\mathsf{h}/2 - 3\eta$, where η and h are synchronous gauge fields in the Fourier space) as

$$\delta_c' + kv_c + \frac{\mathsf{h}'}{2} = \mathcal{H}\beta(a)\frac{\rho_{\rm de}}{\rho_c}(\delta_c - \delta_{\rm de}), \tag{22}$$

$$v_c' + \mathcal{H}v_c = 0, \tag{23}$$

$$\delta_{\rm de}' + 3\mathcal{H}(c^2_{s,\rm de} - w_{\rm de})\delta_{\rm de} + (1+w_{\rm de})\left(kv_{\rm de} + \frac{\mathsf{h}'}{2}\right) + 3\mathcal{H}[3\mathcal{H}(1+w_{\rm de})(c^2_{s,\rm de} - w_{\rm de}]\frac{v_{\rm de}}{k} + 3\mathcal{H}w_{\rm de}'\frac{v_{\rm de}}{k} = 3\mathcal{H}^2\beta(a)c^2_{s,\rm de} - w_{\rm de}\frac{v_{\rm de}}{k}, \tag{24}$$

$$v_{\rm de}' + \mathcal{H}(1 - 3c^2_{s,\rm de})v_{\rm de} - \frac{k\delta_{\rm de}c^2_{s,de}}{(1+w_{\rm de})} = \frac{\mathcal{H}\beta(a)}{(1+w_{\rm de})}[v_c - (1+c^2_{s,\rm de})v_{\rm de}]. \tag{25}$$

It may be noted that although the interaction term in Eq. (21) is similar to that used in [144], the perturbation equations [Eqs. (22)–(25)] are different from those in [144] as we have not considered vacuum energy with $w_{\rm de} = -1$. For the same reason the initial conditions, to follow, are also different in our case. For a detailed discussion on perturbation equations in an inhomogeneous vacuum scenario, we refer to [17,19,42,69,178]. The coupled differential equations [Eqs. (22)–(25)] are solved with $k = 0.1h$ Mpc^{-1} and the adiabatic initial conditions using CAMB. Using the gauge-invariant quantity [161,166,167,174,176] $\zeta_A = (-\psi - \mathcal{H}\frac{\delta\rho_A}{\rho_A'})$ and relative entropy perturbation $S_{AB} = 3(\zeta_A - \zeta_B)$, the adiabatic initial conditions for δ_c, $\delta_{\rm de}$ in presence of interaction are obtained respectively as

[1]Available at: https://camb.info

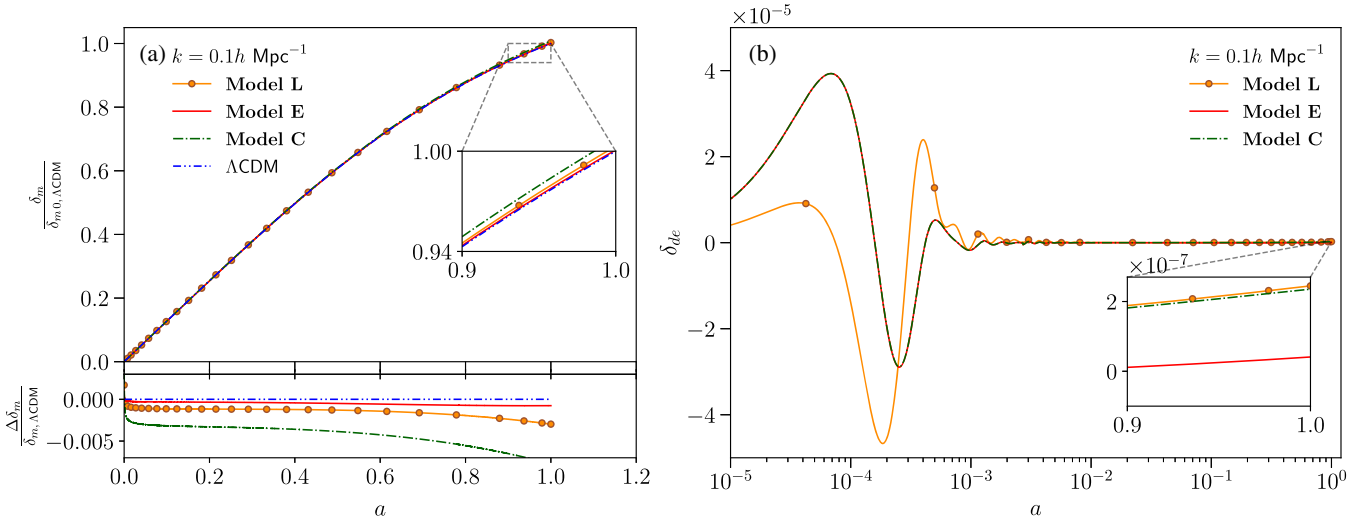

FIG. 2. (a) Plot of Upper panel: the matter density contrast $\frac{\delta_m}{\delta_{m0,\Lambda CDM}}$ and lower panel: fractional growth rate is defined as $\frac{\Delta\delta_m}{\delta_{m,\Lambda CDM}} = (1 - \frac{\delta_m}{\delta_{m,\Lambda CDM}})$ relative to the ΛCDM model against a. The origin on the x-axis represents 10^{-5}. (b) Plot of the dark energy density fluctuation, δ_{de} against a in logarithmic scale for $k = 0.1h$ Mpc^{-1}. The solid line with solid circles represents Model L, solid line represents Model E and dashed-dot line represents Model C while the dashed-dot-dot line is for ΛCDM. The inset shows the zoomed-in portion from $a = 0.9$ to $a = 1.0$.

$$\delta_{ci} = \left[3 + \frac{\rho_{de}}{\rho_c}\beta(a)\right]\frac{\delta_\gamma}{3(1+w_\gamma)}, \tag{26a}$$

$$\delta_{dei} = [3(1+w_{de}) - \beta(a)]\frac{\delta_\gamma}{3(1+w_\gamma)}, \tag{26b}$$

Here, δ_γ is the density fluctuation of photons. As can be seen from Eq. (23), there is no momentum transfer in the DM frame, hence initial value for v_c is set to zero ($v_{ci} = 0$) [63,160,166,167]. The initial value for the dark energy velocity, v_{de} is assumed to be same as the initial photon velocity, $v_{dei} = v_{\gamma i}$. To avoid the instability in dark energy perturbations due to the propagation speed of pressure perturbations, we have set $c^2_{s,de} = 1$ [160,179–182].

Figure 2(a) shows the variation of the density contrast, $\delta_m = \delta\rho_m/\rho_m$ for the cold dark matter (c) taken together and the baryonic matter (b) against a for Model L, Model E, and Model C along with the ΛCDM model. For a better comparison with the ΛCDM model, δ_m is scaled by $\delta_{m0} = \delta_m(a = 1)$ of ΛCDM.[2] As can be seen from the Fig. 2(a), the growth of density fluctuation δ_m is similar in all the model at early times. The effect of interaction comes into play at late time. The late-time growth of δ_m [inset of 2(a)] shows that Model E agrees well with the ΛCDM model, whereas Model L and Model C grow to a little higher value. Figure 2(b) shows the variation of the dark energy density contrast δ_{de} for Model L, Model E and Model C. At early time, δ_{de} oscillates and then decays to very small values. In Model C, the early time evolution of δ_{de} is similar to Model E while the late time evolution is similar to Model L. To understand the differences among the three models and the ΛCDM model, we have shown the fractional matter density contrast, $\frac{\Delta\delta_m}{\delta_{m,\Lambda CDM}} = (1 - \frac{\delta_m}{\delta_{m,\Lambda CDM}})$ in the lower panel of Fig. 2(a). It is clearly seen that, δ_m for Model E evolves close to the ΛCDM model.

A. Effect on CMB temperature, matter power spectrum and $f\sigma_8$

It is necessary to have an insight into other physical quantities like the CMB temperature spectrum, matter power spectrum and the logarithmic growth of matter perturbation, to differentiate the interacting models. The CMB temperature power spectrum is given as

$$C^{TT}_\ell = \frac{2}{k}\int k^2 dk P_\zeta(k)\Delta^2_{T\ell}(k), \tag{27}$$

where ℓ is the multipole index, $P_\zeta(k)$ is the primordial power spectrum, $\Delta_{T\ell}(k)$ is the temperature transfer function and T represents the temperature. For a detailed analysis on the CMB spectrum we refer to [183–185]. The matter power spectrum is written as

$$P(k,a) = A_s k^{n_s} T^2(k) D^2(a), \tag{28}$$

where A_s is the scalar primordial power spectrum amplitude, n_s is the spectral index, $T(k)$ is the matter transfer function and $D(a) = \frac{\delta_m(a)}{\delta_m(a=1)}$ is the normalized density contrast. For a detailed description we refer to [185]. Both C^{TT}_ℓ and $P(k,a)$ are computed numerically using

[2]The origin on the x-axis is actually 10^{-5}

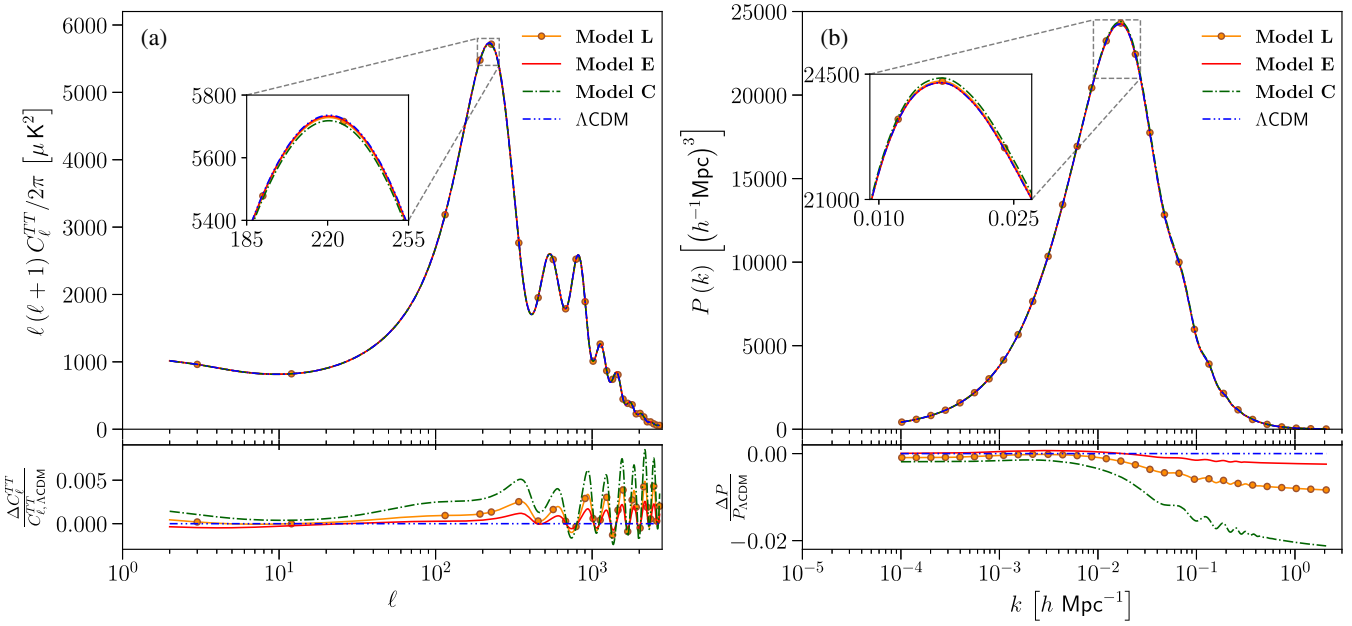

FIG. 3. Upper panel: (a) Plot of CMB temperature power spectrum in units of $\mu\mathrm{K}^2$ with the multipole index ℓ in logarithmic scale. (b) Plot of matter power spectrum $P(k)$ in units of $(h^{-1}\ \mathrm{Mpc}^3)$ with wave number k in units of $h\ \mathrm{Mpc}^{-1}$. Lower panel: plot of fractional change in the temperature spectrum, $\frac{\Delta C_\ell^{TT}}{C_{\ell,\Lambda\mathrm{CDM}}^{TT}} = (1 - \frac{C_\ell^{TT}}{C_{\ell,\Lambda\mathrm{CDM}}^{TT}})$ and the fractional change in matter power spectrum, $\frac{\Delta P}{P_{\Lambda\mathrm{CDM}}} = (1 - \frac{P}{P_{\Lambda\mathrm{CDM}}})$. For both the panels, the solid line with solid circles represents Model L, solid line represents Model E, and dashed-dot line represents Model C while the dashed-dot-dot line is for ΛCDM at $a = 1$. The inset shows the zoomed-in versions of the peaks.

CAMB. The values of power spectrum amplitude, $A_s = 2.100549 \times 10^{-9}$ and spectral index, $n_s = 0.9660499$ are taken from *Planck* 2018 data [6].

Figure 3 shows the temperature and matter power spectrum for Model L, Model E, Model C, and ΛCDM at $a = 1$. In Model L and Model C, more matter content results in lower amplitude of the first peak of the CMB spectrum compared to the ΛCDM model. The lower panel of Fig. 3(a), shows the fractional change $(= \Delta C_\ell^{TT}/C_{\ell,\Lambda\mathrm{CDM}}^{TT})$ in C_ℓ^{TT}. It is seen from the lower panel of Fig. 3(a), that the low-ℓ modes of Model E increases through the integrated Sachs-Wolfe (ISW) effect. More matter content also increases the matter power spectrum compared to the ΛCDM model. The deviations from the ΛCDM model are prominent for the smaller modes. These features are clear from the lower panel of Fig. 3(b), which shows the fractional change in matter power spectrum, $\Delta P/P_{\Lambda\mathrm{CDM}}$ of the interacting models relative to the ΛCDM model.

The presence of the interaction modifies the logarithmic growth rate which helps in differentiating between the models even better. The growth rate is the logarithmic derivative of the density fluctuation of matter (baryon and CDM) and is written as

$$f(a) = \frac{d\ln\delta_m}{d\ln a} = a\frac{d}{da}\left(\frac{\delta\rho_m}{\rho_m}\right). \tag{29}$$

Since, $\delta\rho_m = (\delta_c\rho_c + \delta_b\rho_b)$, δ_b being the baryon density fluctuation, in presence of interaction the growth rate [115] will be

$$f(a) = a\left(\frac{\delta_{c,a}\rho_c + \delta_{b,a}\rho_b}{\delta_m\rho_m} - \frac{aQ\delta_c}{\delta_m\rho_m} - \frac{aQ}{\rho_m}\right), \tag{30}$$

where "$_{,a}$" denotes the derivative with respect to the scale factor a and Q is given by Eq. (21). It must be noted that the last two terms involving interaction Q is introduced in Eq. (30) via the evolution of ρ_c [Eqs. (4)]. We have calculated the growth rate, f for the different models using CAMB.

Observationally the galaxy density fluctuation, δ_g is measured, which in turn gives the matter density fluctuation, δ_m as $\delta_g = b\delta_m$, where $b \in [1, 3]$ is the bias parameter. This δ_m is used to calculate the logarithmic growth rate, f. Thus, f is sensitive to b and is not a very reliable quantity. A more dependable observational quantity is defined as the product $f(a)\sigma_8(a)$ [186], where $\sigma_8(a)$ is the root-mean-square (rms) mass fluctuations within the sphere of radius $R = 8h^{-1}$ Mpc. The mean-square mass fluctuation is given by

$$\sigma^2(R, z) = \frac{1}{2\pi^2}\int k^3 P(k, z) W(kR)^2 \frac{dk}{k} \tag{31}$$

where $P(k, z)$ is the power spectrum given in Eq. (28) and $W(kR)$ is the top-hat window function given by

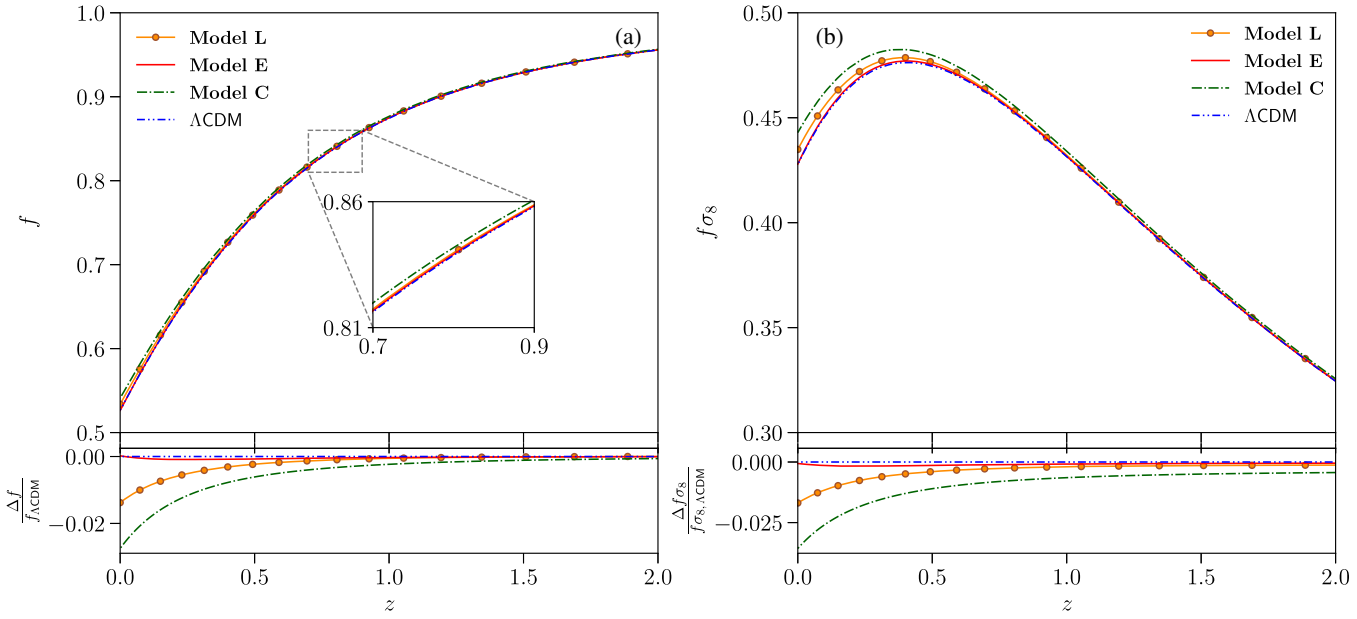

FIG. 4. Upper panel: plot of (a) linear growth rate f and (b) $f\sigma_8$ against redshift z. The inset shows the zoomed-in portion from $z = 0.7$ to $z = 0.9$. Lower panel: plot of fractional change in the temperature spectrum, $\frac{\Delta f}{f_{\Lambda\mathrm{CDM}}} = (1 - \frac{f}{f_{\Lambda\mathrm{CDM}}})$ and the fractional change in matter power spectrum, $\frac{\Delta f\sigma_8}{f\sigma_{8,\Lambda\mathrm{CDM}}} = (1 - \frac{f\sigma_8}{f\sigma_{8,\Lambda\mathrm{CDM}}})$. For both the panels, the solid line with solid circles represents Model L, solid line represents Model E, and dashed-dot line represents Model C while the dashed-dot-dot line is for ΛCDM.

$$W(kR) = 3\left[\frac{\sin(kR)}{(kR)^3} - \frac{\cos(kR)}{(kR)^2}\right]. \tag{32}$$

When the size of the filter is $R = 8h^{-1}$ Mpc, $\sigma^2(R, z) \equiv \sigma_8^2(z)$. The rms linear density fluctuation is also written as $\sigma_8(a) = \sigma_8(1)\frac{\delta_m(a)}{\delta_m(1)}$, where $\sigma_8(1)$ and $\delta_m(1)$ are the values at $a = 1$, and f and $\sigma_8(1)$ for the different models are obtained from Eq. (30) and (31) using our modified version of CAMB. The combination $f\sigma_8$ is written as

$$f\sigma_8(a) \equiv f(a)\sigma_8(a) = \sigma_8(1)\frac{a}{\delta_m(1)}\frac{d\delta_m}{da}. \tag{33}$$

The logarithmic growth rates, f and $f\sigma_8$ are independent of the wave number k for smaller redshift, z, so only the domain $z = 0$ to $z = 2$ is considered here. The redshift, z and the scale factor a are related as $z = \frac{a_0}{a} - 1$, a_0 being the present value (taken to be unity). The difference in the models is magnified in the f and $f\sigma_8$ analysis. As can be seen from Fig. 4, growth rates (f) and $f\sigma_8$ are different for the different models in the recent past. The differences due to the evolution of interaction are seen in f and $f\sigma_8$. Both Model L and Model C have slightly higher values of f and $f\sigma_8$ at $z = 0$, compared to the value obtained from the ΛCDM model. For Model E and the ΛCDM model, the values of f and $f\sigma_8$ are same at $z = 0$. When the energy transfer rates were different in the recent past, Model E had a slightly larger value of f and $f\sigma_8$ (compared to the ΛCDM model) when the interaction was nonzero. The fractional changes in growth rate ($\Delta f/f_{\Lambda\mathrm{CDM}}$) and $f\sigma_8$ ($\Delta f\sigma_8/f\sigma_{8,\Lambda\mathrm{CDM}}$) of the interacting models relative to the ΛCDM model are shown in the lower panels. The difference among the three models is distinctly seen.

IV. OBSERVATIONAL CONSTRAINTS

In this section, Model L, Model E, and Model C are tested against observational datasets like the CMB, BAO, Supernovae, and RSD data by using the Markov Chain Monte Carlo (MCMC) analysis of the publicly available, efficient MCMC simulator CosmoMC[3] [187,188]. The datasets and the methodology are discussed in the Appendix A. The datasets are used to constrain the nine-dimensional parameter space given as

$$P \equiv \{\Omega_b h^2, \Omega_c h^2, 100\theta_{MC}, \tau, \beta_0, w_0, w_1, \ln(10^{10}A_s,)n_s\}, \tag{34}$$

where $\Omega_b h^2$ is the baryon density, $\Omega_c h^2$ is the cold dark matter density, θ_{MC} is the angular acoustic scale, τ is the optical depth, β_0, w_0 and w_1 are the free model parameters, A_s is the scalar primordial power spectrum amplitude and n_s is the scalar spectral index. The parameter space, P, for all the three models, is explored for the flat prior ranges given in Table II. We allowed the prior of β_0 to cross the

[3]Available at: https://cosmologist.info/cosmomc/

TABLE II. Prior ranges of nine independent parameters used in the CosmoMC analysis.

Parameter	Prior
$\Omega_b h^2$	[0.005, 0.1]
$\Omega_c h^2$	[0.001, 0.99]
$100\theta_{MC}$	[0.5, 10]
τ	[0.01, 0.8]
β_0	$[-1.0, 1.0]$
w_0	$[-0.9999, -0.3333]$
w_1	[0.005, 1.0]
$\ln(10^{10}A_s)$	[1.61, 3.91]
n_s	[0.8, 1.2]

zero and set the prior of w_0 and w_1 such that such that $w_{\rm de}$ is always in the quintessence region.

A. Model L

For Model L, the marginalized values with errors at 1σ (68% confidence level) of the nine free parameters and three derived parameters, H_0, Ω_m and σ_8, are listed in Table III. Henceforth, the 1D marginalized values given in the tables will be referred to as mean values. The correlations between the model parameters (β_0, w_0, w_1) and the derived parameters (H_0, Ω_m, σ_8) and their marginalized contours are shown in Fig. 5. The contours contain 1σ region (68% confidence level) and 2σ region (95% confidence level). When only the *Planck* data is considered, the mean value of the coupling parameter, $\beta_0 (= 0.00788^{+0.00815+0.0158}_{-0.00815-0.0162})$, is positive with zero in the 1σ region indicating energy transfers from DM to DE. The parameters $w_0 (< -0.909 < -0.800)$ and $w_1 (< 0.174 < 0.365)$ remain unconstrained even in the 2σ region. For other parameters, the mean values are compared with their ΛCDM counterparts from the *Planck* estimation [6]. The Hubble expansion rate, H_0, is obtained at a value lower than 67.36 ± 0.54 in $\mathrm{km\,s^{-1}\,Mpc^{-1}}$, as obtained for the ΛCDM model [6]. Though the mean value is lower than that obtained from the *Planck* estimate, the presence of high error bars results in 3.5σ tension with the local measurement as $H_0 = 74.03 \pm 1.42$ $\mathrm{km\,s^{-1}\,Mpc^{-1}}$. The value of the late time clustering amplitude (σ_8) is skewed toward the value, $\sigma_8 = 0.77^{+0.04}_{-0.03}$, as obtained by the galaxy cluster counts using thermal Sunyaev-Zel'dovich (tSZ) signature [6,189]. Thus, *Planck* data alone alleviates the σ_8 tension in the Model L. Figure 5 highlights the positive correlation between H_0 and σ_8 and strong negative correlations of Ω_m with H_0 and σ_8. The parameter w_0 has negative correlations with w_1, H_0 and σ_8 and positive correlation with Ω_m. The coupling parameter (β_0) is uncorrelated to the others.

Addition of the BAO to the *Planck* data, increases the value of β_0 to $0.00814^{+0.00755+0.0146}_{-0.00755-0.0151}$ with zero outside the 1σ region. The *Planck* and BAO combination cannot constrain the parameters w_0 and w_1. The mean value of the Hubble parameter increases considerably but is still smaller than the corresponding value for ΛCDM, $H_0 = 67.66 \pm 0.42$ in $\mathrm{km\,s^{-1}\,Mpc^{-1}}$ in the 1σ region. The considerable decrease in error bar increased the H_0 tension to $\sim 4\sigma$. The values of Ω_m decreases and σ_8 increases and are higher than the ΛCDM counterpart ($\Omega_m = 0.3111 \pm 0.0056$ and $\sigma_8 = 0.8102 \pm 0.006$) in the 1σ region. Thus, addition of the BAO data to the *Planck* data restores the σ_8 tension ($\sim 0.79\sigma$) in Model L. The combination also lowers the error regions substantially.

Interestingly, addition of $f\sigma_8$ to the *Planck* data changes the parameter mean values in the similar fashion like the *Planck* and BAO combination but the error bars become higher. This is also clear from Fig. 5. The mean value of $\beta_0 (= 0.00752^{+0.00757+0.0145}_{-0.00757-0.0151})$ is smaller the *Planck* and

TABLE III. Observational constraints on the nine dependent model parameters with three derived parameters separated by a horizontal line and the error bars correspond to 68% confidence level for Model L, using different observational datasets.

Parameter	Planck	Planck + $f\sigma_8$	Planck + BAO	Planck + BAO+ Pantheon	Planck + BAO+ Pantheon + $f\sigma_8$
$\Omega_b h^2$	0.022362 ± 0.000168	0.022483 ± 0.000163	0.022487 ± 0.000156	0.022500 ± 0.000154	0.022542 ± 0.000152
$\Omega_c h^2$	0.12005 ± 0.00129	0.11853 ± 0.00117	0.11848 ± 0.00102	0.118381 ± 0.000977	0.117838 ± 0.000927
$100\theta_{MC}$	1.040773 ± 0.000326	1.040938 ± 0.000316	1.040951 ± 0.000315	1.040954 ± 0.000316	1.041007 ± 0.000313
τ	0.05475 ± 0.00773	$0.05641^{+0.00705}_{-0.00794}$	$0.05732^{+0.00701}_{-0.00787}$	$0.05707^{+0.00691}_{-0.00777}$	0.05791 ± 0.00760
β_0	0.00788 ± 0.00815	0.00752 ± 0.00757	0.00814 ± 0.00755	0.00859 ± 0.00745	0.00818 ± 0.00731
w_0	< -0.909	< -0.976	< -0.968	< -0.980	< -0.985
w_1	< 0.174	< 0.0672	< 0.0707	< 0.0623	< 0.0500
$\ln(10^{10}A_s)$	3.0489 ± 0.0149	3.0489 ± 0.0147	3.0512 ± 0.0148	3.0507 ± 0.0145	3.0512 ± 0.0146
n_s	0.96330 ± 0.00444	0.96672 ± 0.00436	0.96674 ± 0.00413	0.96690 ± 0.00418	0.96818 ± 0.00412
H_0 [$\mathrm{km\,s^{-1}\,Mpc^{-1}}$]	$63.98^{+2.45}_{-1.47}$	$66.93^{+1.04}_{-0.719}$	$66.770^{+0.792}_{-0.602}$	$67.179^{+0.579}_{-0.521}$	67.596 ± 0.524
Ω_m	$0.3507^{+0.0157}_{-0.0292}$	$0.31643^{+0.00846}_{-0.0116}$	$0.31778^{+0.00681}_{-0.00832}$	0.31368 ± 0.00632	0.30871 ± 0.00598
σ_8	$0.7825^{+0.0228}_{-0.0141}$	$0.8027^{+0.0102}_{-0.00836}$	$0.8020^{+0.0104}_{-0.00892}$	0.80541 ± 0.00862	0.80560 ± 0.00803

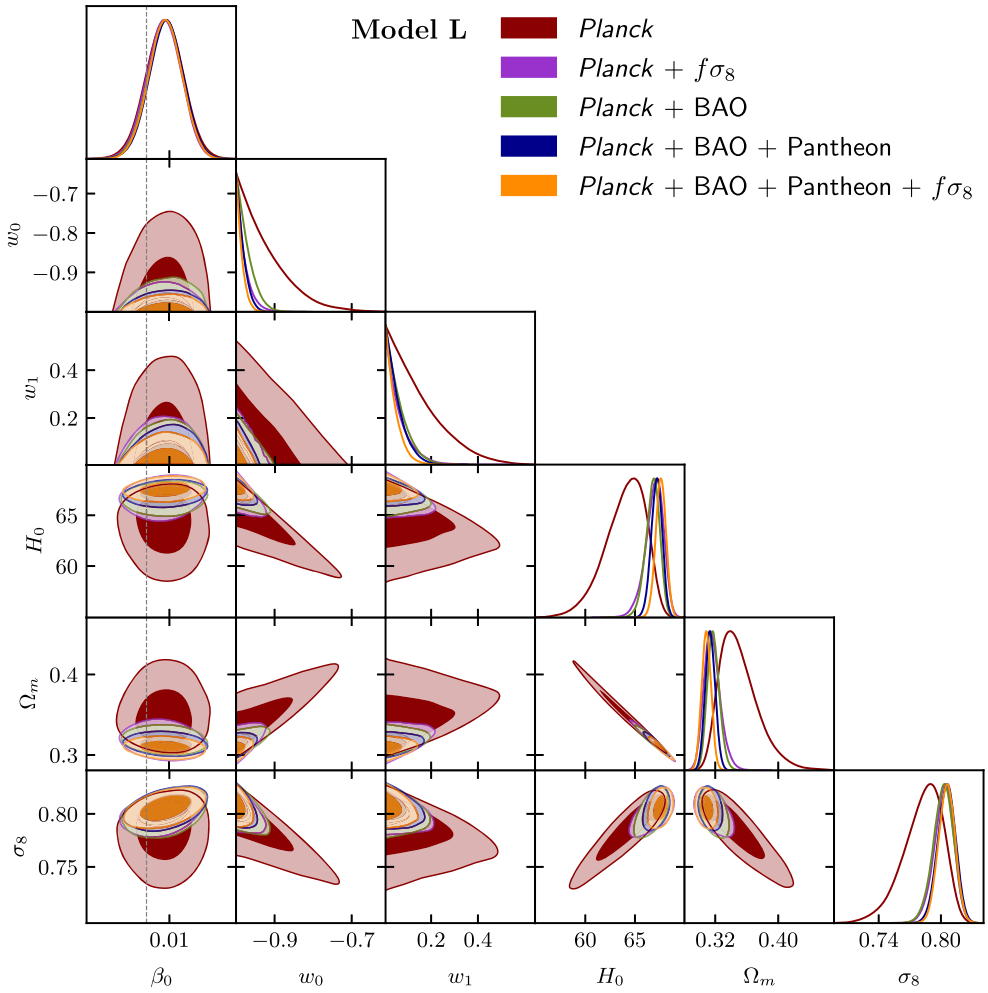

FIG. 5. Plot of 1-dimensional marginalized posterior distributions and 2-dimensional marginalized constraint contours on the parameters of Model L containing 68% and 95% probability. The dashed line represents the $\beta_0 = 0$ value.

BAO combination. Clearly, addition of the $f\sigma_8$ data restores the σ_8 tension in Model L.

Addition of the BAO and Pantheon to the *Planck* data, increases the mean value of $\beta_0 (= 0.00859^{+0.00745+0.0145}_{-0.00745-0.0148})$ with zero in the 2σ region. The parameters w_0 and w_1 still remain unconstrained. The combination increases the H_0 mean value but is still slightly smaller than the fiducial ΛCDM value. The central value of Ω_m at the present epoch remains slightly larger whereas σ_8 remains slightly smaller than the ΛCDM case. Clearly, the σ_8 tension is restored.

Combining $f\sigma_8$ data with *Planck*, BAO and Pantheon lowers the mean values of both Ω_m and σ_8 but increases the value of H_0 compared to the baseline *Planck* values [6]. Thus, addition of all the datasets worsen the H_0 tension ($\sim 4.2\sigma$) and the σ_8 tension ($\sim 0.87\sigma$). The mean value of $\beta_0 (= 0.00818^{+0.00731+0.0142}_{-0.00731-0.0146})$ decreases slightly with zero in the 2σ region. Although the constraints on w_0 and w_1 tightens, they still remain unconstrained.

Combination of all the datasets significantly reduced the error bars. The parameters, β_0 and w_1 become very weakly correlated with other parameters. However, the correlations among the rest of the parameters remain unchanged.

B. Model E

For Model E, the mean values with 1σ errors of the nine free parameters along with the three derived parameters, H_0, Ω_m and σ_8, are given in Table IV. The correlations of the model parameters (β_0, w_0, w_1) with the derived parameters (H_0, Ω_m, σ_8) and their marginalized contours are shown in Fig. 6. When only *Planck* data is considered, the mean value of $\beta_0 (= 0.0339^{+0.0372+0.0724}_{-0.0372-0.0746})$ is large compared to that in Model L, though $\beta_0 = 0$ remains within the 1σ region. The CPL parameters, $w_0 (< -0.914 < -0.809)$ and $w_1 (< 0.168 < 0.355)$, remain unconstrained even within the 2σ region. The values of H_0 is greater and that of σ_8 is slightly grater whereas Ω_m is slightly lower than those in Model L. Similar to Model L, the discrepancy in the value of H_0 with the local measurement is at 3.5σ. In Model E also, the *Planck* data alleviates the σ_8 tension.

TABLE IV. Observational constraints on the nine dependent model parameters with three derived parameters separated by a horizontal line and the error bars correspond to 68% confidence level for Model E, using different observational datasets.

Parameter	Planck	Planck + $f\sigma_8$	Planck + BAO	Planck + BAO+ Pantheon	Planck + BAO+ Pantheon + $f\sigma_8$
$\Omega_b h^2$	0.022358 ± 0.000165	0.022490 ± 0.000162	0.022489 ± 0.000156	0.022500 ± 0.000152	0.022546 ± 0.000151
$\Omega_c h^2$	0.12008 ± 0.00126	0.11848 ± 0.00117	0.11850 ± 0.00101	0.118405 ± 0.000970	0.117845 ± 0.000909
$100\theta_{MC}$	1.040769 ± 0.000324	1.040941 ± 0.000318	1.040941 ± 0.000313	1.040945 ± 0.000315	1.040999 ± 0.000313
τ	$0.05466^{+0.00699}_{-0.00779}$	$0.05630^{+0.00703}_{-0.00797}$	$0.05704^{+0.00704}_{-0.00792}$	0.05697 ± 0.00749	$0.05778^{+0.00700}_{-0.00790}$
β_0	0.0339 ± 0.0372	0.0395 ± 0.0381	0.0432 ± 0.0376	0.0448 ± 0.0377	0.0446 ± 0.0370
w_0	< -0.914	< -0.977	< -0.969	< -0.981	< -0.985
w_1	<0.168	<0.0645	<0.0707	<0.0604	<0.0489
$\ln(10^{10}A_s)$	3.0486 ± 0.0147	3.0488 ± 0.0148	3.0509 ± 0.0148	3.0507 ± 0.0144	3.0511 ± 0.0146
n_s	0.96315 ± 0.00453	0.96681 ± 0.00434	0.96652 ± 0.00419	0.96672 ± 0.00418	0.96802 ± 0.00404
$H_0[\mathrm{km\,s^{-1}\,Mpc^{-1}}]$	$64.12^{+2.40}_{-1.39}$	$67.00^{+1.02}_{-0.702}$	$66.787^{+0.775}_{-0.600}$	$67.200^{+0.577}_{-0.516}$	67.631 ± 0.516
Ω_m	$0.3492^{+0.0149}_{-0.0282}$	$0.31569^{+0.00834}_{-0.0114}$	$0.31765^{+0.00678}_{-0.00812}$	$0.31353^{+0.00590}_{-0.00658}$	0.30842 ± 0.00588
σ_8	$0.7836^{+0.0221}_{-0.0138}$	$0.80265^{+0.00992}_{-0.00800}$	$0.8019^{+0.0102}_{-0.00866}$	0.80539 ± 0.00830	0.80573 ± 0.00774

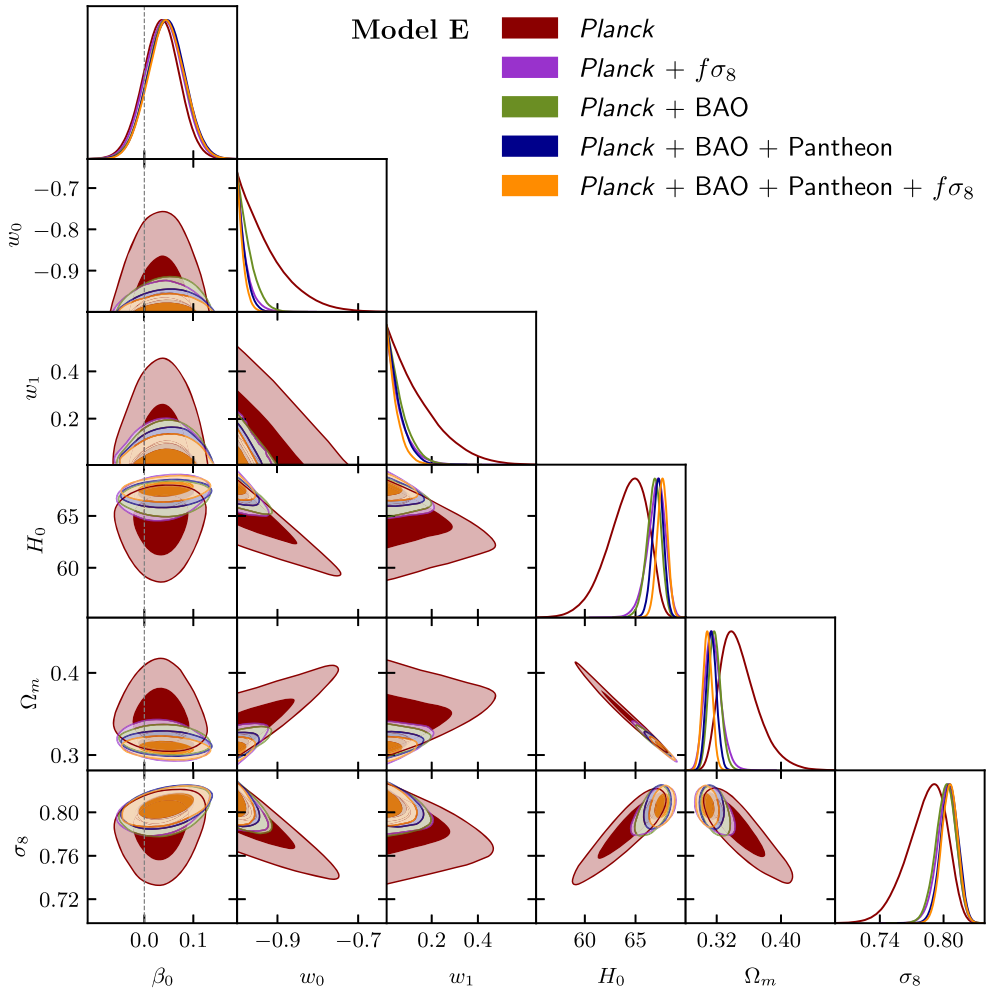

FIG. 6. Plot of 1-dimensional marginalized posterior distributions and 2-dimensional marginalized constraint contours on the parameters of Model E containing 68% and 95% probability. The dashed line represents the $\beta_0 = 0$ value.

TABLE V. Observational constraints on the nine dependent model parameters with three derived parameters separated by a horizontal line and the error bars correspond to 68% confidence level for Model C, using different observational datasets.

Parameter	Planck	Planck + $f\sigma_8$	Planck + BAO	Planck + BAO+ Pantheon	Planck + BAO+ Pantheon + $f\sigma_8$
$\Omega_b h^2$	0.022358 ± 0.000164	0.022482 ± 0.000164	0.022487 ± 0.000156	0.022499 ± 0.000151	0.022545 ± 0.000152
$\Omega_c h^2$	0.12007 ± 0.00128	0.11854 ± 0.00118	0.11849 ± 0.00100	0.118388 ± 0.000977	0.117824 ± 0.000935
$100\theta_{MC}$	1.040772 ± 0.000322	1.040939 ± 0.000321	1.040947 ± 0.000314	1.040954 ± 0.000312	1.041011 ± 0.000311
τ	0.05491 ± 0.00757	$0.05638^{+0.00708}_{-0.00788}$	$0.05718^{+0.00685}_{-0.00788}$	0.05730 ± 0.00751	$0.05800^{+0.00707}_{-0.00790}$
β_0	0.00624 ± 0.00673	0.00621 ± 0.00626	0.00696 ± 0.00629	0.00708 ± 0.00631	0.00693 ± 0.00615
w_0	< -0.907	< -0.977	< -0.969	< -0.981	< -0.985
w_1	< 0.174	< 0.0681	< 0.0728	< 0.0610	< 0.0511
$\ln(10^{10}A_s)$	3.0493 ± 0.0146	3.0489 ± 0.0147	3.0511 ± 0.0146	3.0511 ± 0.0144	3.0514 ± 0.0147
n_s	0.96331 ± 0.00444	0.96670 ± 0.00435	0.96670 ± 0.00416	0.96695 ± 0.00415	0.96823 ± 0.00414
$H_0[\mathrm{km\,s^{-1}\,Mpc^{-1}}]$	$63.93^{+2.51}_{-1.44}$	$66.93^{+1.03}_{-0.714}$	$66.759^{+0.795}_{-0.594}$	$67.187^{+0.581}_{-0.516}$	$67.606^{+0.552}_{-0.493}$
Ω_m	$0.3513^{+0.0153}_{-0.0299}$	$0.31643^{+0.00843}_{-0.0115}$	$0.31789^{+0.00671}_{-0.00832}$	0.31361 ± 0.00631	0.30860 ± 0.00605
σ_8	$0.7821^{+0.0232}_{-0.0140}$	$0.8026^{+0.0100}_{-0.00823}$	$0.8020^{+0.0104}_{-0.00879}$	0.80558 ± 0.00856	0.80564 ± 0.00807

The distinguishing feature of Model E is that the mean value of β_0 is greater than that obtained in Model L for all the dataset combinations.

Addition of the BAO to the *Planck* data, increases the mean value of $\beta_0 (= 0.0432^{+0.0376+0.0733}_{-0.0376-0.0744})$ with zero allowed in the 2σ region. The parameters w_0 and w_1 remain unconstrained. The mean value of H_0 increases considerably but is still smaller than the corresponding value for ΛCDM. The values of Ω_m decreases and σ_8 increases and are higher than the ΛCDM counterpart. The addition of BAO data to *Planck* data restores the H_0 ($\sim 4\sigma$) and σ_8 ($\sim 0.77\sigma$) tensions in Model E. The combination also lowers the error bars considerably.

Similar to Model L, addition of $f\sigma_8$ to the *Planck* data changes the parameter mean values like the Planck + BAO combination but the error bars still remain a little higher. This is also clear from Fig. 6. The mean value of $\beta_0 (= 0.0395^{+0.0381+0.0735}_{-0.0381-0.0750})$ is slightly smaller than the Planck + BAO combination. The H_0 and σ_8 tensions are restored on addition of $f\sigma_8$ to the *Planck* data.

Combining BAO and Pantheon with *Planck* data increases the mean value of $\beta_0 (= 0.0448^{+0.0377+0.0738}_{-0.0377-0.0733})$ and $\beta_0 = 0$ is within the 2σ region. The Planck + BAO + Pantheon results in a very small change in the mean values of the parameters along with reduced error bars. The mean values of H_0 and σ_8 increase and Ω_m decreases relative to the Planck + BAO combination. Again, the σ_8 tensions are not alleviated.

Addition of $f\sigma_8$ to the combination Planck + BAO+ Pantheon, increases the mean value of H_0 slightly and decreases the mean value of Ω_m very slightly keeping σ_8 almost unchanged. The mean value of $\beta_0 (= 0.0446^{+0.0370+0.0724}_{-0.0370-0.0726})$ decreases slightly with zero in the 2σ region. Clearly, the addition of datasets do not improve the H_0 and σ_8 tension in Model E. Addition of the datasets significantly reduces the error bars. The correlations between the parameters for Model E remain same as in Model L.

C. Model C

The mean values of the parameters with 1σ errors for Model C are given in Table V. In Table V, the mean values and 1σ errors of the three derived parameters, H_0, Ω_m and σ_8, are also quoted. The correlations between the model parameters (β_0, w_0, w_1) and the derived parameters (H_0, Ω_m, σ_8) along with their marginalized contours are shown in Fig. 7. The parameter values of Model C are very close to those of Model L and they respond to the datasets in the similar fashion as well. Similar to Model L and Model E, H_0 tension is at $\sim 4\sigma$ and only the *Planck* data alleviates the σ_8 tension in Model C whereas consideration of other datasets restore the tension. The main difference is that the mean values of β_0 in Model C is slightly smaller than that in Model L. These features are clearly seen from Table V.

Tension in the H_0 parameter: Dark energy interacting with dark matter is a plausible scenario to resolve the H_0 tension. When $Q > 0$, energy flows from dark matter to dark energy, and we have less dark matter in the present epoch than in the uncoupled case. The locations and heights of the peaks and troughs in the CMB anisotropy depend on the combination $\Omega_m h^2$ of the present epoch. Since baryon energy density remains unaffected by the interaction, any change in the matter (which is a combination of baryonic matter and dark matter) density comes from the dark matter density. For low matter density with fixed H_0, the heights of the CMB peaks are higher (for details we refer to [185]). So a model with less Ω_c at the present epoch will need to have a higher value of H_0 so as to keep the heights of the CMB peaks unaltered. Thus a

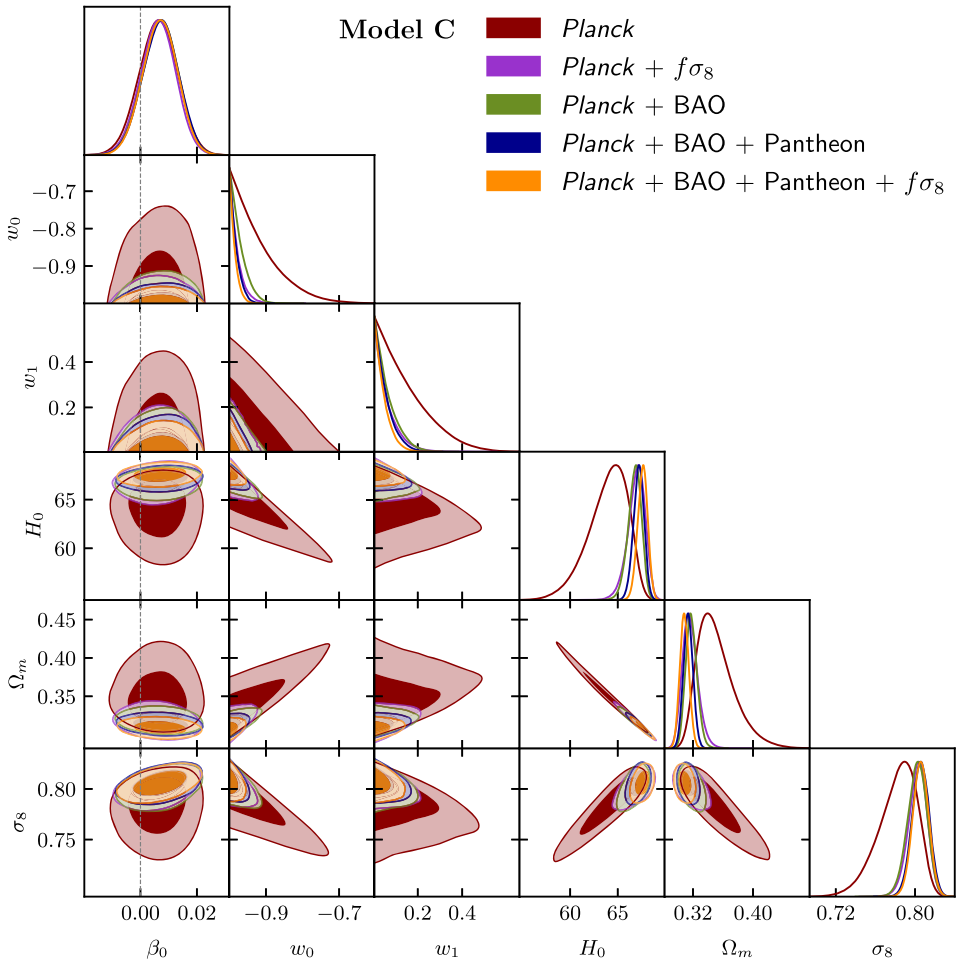

FIG. 7. Plot of 1-dimensional marginalized posterior distributions and 2-dimensional marginalized constraint contours on the parameters of Model C containing 68% and 95% probability. The dashed line represents the $\beta_0 = 0$ value.

larger value of H_0 will be obtained when constrained with the CMB data, which will reconcile the H_0 tension. It may be noted that in the present work, the uncoupled case is not the ΛCDM model and H_0 tension is not alleviated.

V. BAYESIAN EVIDENCE

Finally, we aim to investigate which one of Model L, Model E, and Model C is statistically favored by the observational data. The Bayesian evidence or more precisely, the logarithm of the Bayes factor, $\ln B_{ij}$ given in Eq. (B3), for each of the three models is calculated. Here, i corresponds to Model L, Model E, and Model C for each of the dataset combination, j corresponds to the reference model, M_j. The details on the Bayes factor, B_{ij}, are discussed in Appendix B. The fiducial ΛCDM model is considered to be the reference model, and therefore, a negative value ($\ln B_{ij} < 0$) indicates a preference for the ΛCDM model. The logarithmic Bayes factor, $\ln B_{ij}$, is calculated directly from the MCMC chains using the publicly available cosmological package

TABLE VI. The values of $\ln B_{ij}$, where j is the ΛCDM model and i is the interacting model. A negative sign indicates M_j is favored over M_i. The $|\ln B_{ij}|$ values are compared with Table VIII. The column $\Delta \ln B_{ij}$ corresponds to the comparison of Model L and Model E with Model C.

Model	Dataset	$\ln B_{ij}$	$\Delta \ln B_{ij}$
Model L	Planck	−8.843	−2.244
	Planck + $f\sigma_8$	−11.410	−2.245
	Planck + BAO	−10.610	−2.187
	Planck + BAO + Pantheon	−11.354	−2.104
	Planck + BAO + Pantheon + $f\sigma_8$	−11.977	−2.328
Model E	Planck	−7.233	−0.633
	Planck + $f\sigma_8$	−9.730	−0.566
	Planck + BAO	−9.047	−0.624
	Planck + BAO + Pantheon	−9.733	−0.483
	Planck + BAO + Pantheon + $f\sigma_8$	−10.192	−0.542
Model C	Planck	−6.599	0.0
	Planck + $f\sigma_8$	−9.164	0.0
	Planck + BAO	−8.423	0.0
	Planck + BAO + Pantheon	−9.250	0.0
	Planck + BAO + Pantheon + $f\sigma_8$	−9.650	0.0

MCEvidence[4] [190,191]. The computed values of $\ln B_{ij}$ for Model L, Model E and Model C are summarized in Table VI. From Table VI, it is clear that the ΛCDM model is preferred over the interacting models by all the dataset combinations. However, the motive is to assess if there is any observationally preferable evolution stage when the interaction is significant. As can be seen from the relative differences of $|\ln B_{ij}|$ (values corresponding to column $\Delta \ln B_{ij}$) in Table VI), when compared with Model C, Model L is strongly disfavored while Model E is weakly disfavored by observational data over Model C.

VI. SUMMARY AND DISCUSSION

The present work deals with the matter perturbations in a cosmological model where the dark energy has an interaction with the dark matter. We investigate the possibility whether the coupling parameter between the two dark components can evolve. We have considered two new examples, (a) the interaction is a recent phenomenon [Model L; Eq. (8a)], and (b) the interaction is an early phenomenon [Model E; Eq. (8b)] and compared them with the normally talked about model where the coupling is a constant [Model C; Eq. (8c)], in the context of density perturbations. The results are compared with the standard ΛCDM model as well. The rate of energy transfer is proportional to the dark energy density, ρ_{de} and energy flows from dark matter to dark energy. The interaction term is given by Eq. (21). We have also considered the dark energy to have a dynamical EoS parameter, w_{de} being given by the CPL parametrization (Eq. (9)).

We have worked out a detailed perturbation analysis of the models in the synchronous gauge and compared them with each other. The background dynamics of the three interacting models are almost the same, which is evident from the smallness of the coupling parameter and the domination of dark energy at late times. The signature of the presence of interaction at different epochs for different couplings are noticeable in the perturbation analysis.

In all the three interacting models, the fractional density perturbation of dark matter is marginally higher than that in a ΛCDM model, indicating more clumping of matter. From the CMB temperature spectrum, matter power spectrum and the evolution of growth rate, we note that the presence of interaction for a brief period in the evolutionary history (Model E), makes the Universe behave like the ΛCDM model with a slightly higher value of $f\sigma_8$ at the epoch when the interaction prevails. The first part of the present work shows that Model E behaves in a closely similar fashion as the ΛCDM model and leads to the conclusion that Model E performs better than Model L and Model C in describing the evolutionary history of the Universe.

To determine further the evolution stage when the interaction is significant, we have tested the interacting models with the observational datasets. We have tested Model E, Model L, and Model C against the recent observational datasets like CMB, BAO, Pantheon and RSD with the standard six parameters of ΛCDM model along with the three model parameters, β_0, w_0 and w_1. We have obtained the mean value of the coupling parameter, β_0 to be positive, indicating an energy flow from dark matter to dark energy. When only CMB data is used, $\beta_0 = 0$ lies within the 1σ error region while when different combinations of the datasets are used, $\beta_0 = 0$ lies outside the 1σ error region. The priors of w_0 and w_1 are set such that w_{de} remains in the quintessence region. Hence, w_0 and w_1 remain unconstrained. Moreover, for all the three interacting models, the σ_8 tension is alleviated when CMB data is used. Though the estimated parameter values are prior dependent, it can be said conclusively that the CMB data and RSD data are in agreement when the interacting models are considered. Addition of other datasets restore the σ_8 tension in all the three interacting models. However, the tension in H_0 value persists for all the three interacting models.

From the Bayesian evidence analysis, we see that all the three interacting dark energy models are rejected by observational data when compared with the fiducial ΛCDM model. However, a close scrutiny reveals that both Model E and Model C are favored over Model L. Though the Bayesian evidence analysis ever so slightly favors Model C over Model E, the difference is too small to choose a clear winner. Thus, to conclude from the results of the perturbation analysis and observational data we infer that the interaction, if present, is likely to be significant only at some early stage of evolution of the Universe.

ACKNOWLEDGMENTS

The author is indebted to Narayan Banerjee for valuable suggestions and discussions. The author would also like to thank Tuhin Ghosh, Supriya Pan and Ankan Mukherjee for their insightful comments and suggestions.

APPENDIX A: OBSERVATIONAL DATA AND METHODOLOGY

Different observational datasets obtained from the publicly available cosmological probes have been used to constrain the parameters of the interacting models. The datasets used in this work are listed below.

CMB: We considered the cosmic microwave background (CMB) anisotropies data from the latest 2018 data release of the *Planck* collaboration[5] [6,126]. The CMB likelihood consists of the low-ℓ temperature likelihood, C_ℓ^{TT}, the low-ℓ polarization likelihood, C_ℓ^{EE},

[4]Available on GitHub: https://github.com/yabebalFantaye/MCEvidence

[5]Available at: https://pla.esac.esa.int

high-ℓ temperature-polarization likelihood, C_ℓ^{TE}, high-ℓ combined TT, TE, and EE likelihood. The low-ℓ likelihoods span from $2 \leq \ell \leq 29$ and the high-ℓ likelihoods consists of multipole values $\ell \geq 30$ and collectively make the combination *Planck* TT, TE, EE + lowE. For CMB lensing data, the power spectrum of the lensing potential measured by *Planck* collaboration is used. The *Planck* TT, TE, EE + lowE, along with the lensing likelihood (*Planck* TT, TE, EE + lowE + lensing) are denoted as "*Planck*" in the results given in Sec. IV. References [6,126] provide a detailed study of the CMB likelihoods.

BAO: The photon-baryon fluid fluctuations in the early Universe leave their signatures as the acoustic peaks in the CMB anisotropies power spectrum. The anisotropies of baryon acoustic oscillations (BAO) provide tighter constraints on the cosmological parameters [192]. The BAO surveys measure the ratio, D_V/r_d at different effective redshifts. The quantity D_V is related to the comoving angular diameter D_M and Hubble parameter H as

$$D_V(z) = \left[D_M^2(z)\frac{cz}{H(z)}\right]^{1/3}, \tag{A1}$$

and r_d refers to the comoving sound horizon at the end of baryon drag epoch. For the BAO data, three surveys are considered: the 6dF Galaxy Survey (6dFGS) measurements [92] at redshift $z = 0.106$, the Main Galaxy Sample of Data Release 7 of the Sloan Digital Sky Survey (SDSS-MGS) [93] at redshift $z = 0.15$ and the latest Data Release 12 (DR12) of the Baryon Oscillation Spectroscopic Survey (BOSS) of the Sloan Digital Sky Survey (SDSS) III at redshifts $z = 0.38$, 0.51 and 0.61 [9].

Pantheon: We considered the latest "Pantheon" catalogue for the luminosity distance measurements of the Type Ia supernovae (SNe Ia) [4]. The Pantheon sample is the compilation of 276 supernovae discovered by the Pan-STARRS1 Medium Deep Survey at $0.03 < z < 0.65$ and various low redshift and Hubble Space Telescope (HST) samples to give a total of 1048 supernovae data in the redshift range $0.01 < z < 2.3$.

RSD: Redshift-space distortion (RSD) is the cosmological effect where spatial galaxy maps produced by measuring distances from the spectroscopic redshift surveys show an anisotropic galaxy distribution. These galaxy anisotropies arise due to the galaxy recession velocities having components from both the Hubble flow and comoving peculiar velocities from the motions of galaxies and result in the anisotropies of the observed power spectrum. However, additional anisotropies in the power spectrum arise due to incorrect fiducial cosmology, $H(z)$ while converting the relative redshifts to comoving coordinates. The introduction of anisotropies due to incorrect fiducial cosmology is called Alcock-Paczyński (AP) effect [193]. The RSD surveys measure the matter peculiar velocities and provide the galaxy matter density perturbation, δ_g [94]. As mentioned in Sec. III A, the combination $f\sigma_8$ is the widely used quantity to study the growth rate of the matter density perturbation. In the present work, we considered the $f\sigma_8$ data compilation by Nesseris *et al.* [116], Sagredo *et al.* [117] and Skara and Perivolaropoulos [118]. The surveys and the corresponding data points used in this work are shown in Table VII, along with the corresponding fiducial cosmology used by the collaborations to convert redshift to distance in each case. The fiducial cosmology in Table VII is used to correct the AP effect following Macaulay *et al.* [194] as discussed in [117,118]. The RSD measurement is denoted as '$f\sigma_8$' data in the results given in Sec. IV.

The covariance matrices of the data from the WiggleZ [195] and the SDSS-IV [196] surveys are given as

$$\mathbf{C}_{\mathrm{WiggleZ}} = 10^{-3}\begin{pmatrix} 6.400 & 2.570 & 0.000 \\ 2.570 & 3.969 & 2.540 \\ 0.000 & 2.540 & 5.184 \end{pmatrix}, \tag{A2}$$

and

$$\mathbf{C}_{\text{SDSS-IV}} = 10^{-2}\begin{pmatrix} 3.098 & 0.892 & 0.329 & -0.021 \\ 0.892 & 0.980 & 0.436 & 0.076 \\ 0.329 & 0.436 & 0.490 & 0.350 \\ -0.021 & 0.076 & 0.350 & 1.124 \end{pmatrix} \tag{A3}$$

respectively.

To compare the interacting model with the observational data, we calculated the likelihood as

$$\mathcal{L} \propto e^{-\chi^2/2}, \quad \text{where } \chi^2 = \chi^2_{\mathrm{CMB}} + \chi^2_{\mathrm{BAO}} + \chi^2_{\mathrm{Pantheon}} + \chi^2_{f\sigma_8}. \tag{A4}$$

According to Bayes theorem [see Eq. (B1)], the likelihood is the probability of the data given the model parameters. The quantity χ^2 for any dataset is calculated as

$$\chi^2_i = V^i \mathbf{C}^{-1}_{ij} V^j, \tag{A5}$$

where the vector, V^i is written as

$$V^i = \Theta^{\mathrm{obs}}_i - \Theta^{\mathrm{th}}(z_i, P) \tag{A6}$$

with Θ being the physical quantity corresponding to the observational data (*Planck*, BAO, Pantheon, $f\sigma_8$) used, z_i being the corresponding redshift, $\mathbf{C}^{-1}_{ij}$ is the corresponding

TABLE VII. A compilation of $f\sigma_8$ measurements with redshift z and fiducial value of Ω_m from different surveys.

Survey	z	$f\sigma_8(z)$	Ω_m	Refs.
6dFGS + SnIa	0.02	0.428 ± 0.0465	0.3	[197]
SnIa + IRAS	0.02	0.398 ± 0.065	0.3	[198,199]
2MASS	0.02	0.314 ± 0.048	0.266	[199,200]
SDSS-veloc	0.10	0.370 ± 0.130	0.3	[201]
SDSS-MGS	0.15	0.490 ± 0.145	0.31	[202]
2dFGRS	0.17	0.510 ± 0.060	0.3	[203]
GAMA	0.18	0.360 ± 0.090	0.27	[204]
GAMA	0.38	0.440 ± 0.060		[204]
SDSS-LRG-200	0.25	0.3512 ± 0.0583	0.25	[205]
SDSS-LRG-200	0.37	0.4602 ± 0.0378		[205]
BOSS-LOWZ	0.32	0.384 ± 0.095	0.274	[206]
SDSS-CMASS	0.59	0.488 ± 0.060	0.307115	[207]
WiggleZ	0.44	0.413 ± 0.080	0.27	[195]
WiggleZ	0.60	0.390 ± 0.063	$\mathbf{C}_{ij} \rightarrow$ Eq. (A.2)	[195]
WiggleZ	0.73	0.437 ± 0.072		[195]
VIPERS PDR-2	0.60	0.550 ± 0.120	0.3	[208]
VIPERS PDR-2	0.86	0.400 ± 0.110		[208]
FastSound	1.40	0.482 ± 0.116	0.27	[209]
SDSS-IV	0.978	0.379 ± 0.176	0.31	[196]
SDSS-IV	1.23	0.385 ± 0.099	$\mathbf{C}_{ij} \rightarrow$ Eq. (A.3)	[196]
SDSS-IV	1.526	0.342 ± 0.070		[196]
SDSS-IV	1.944	0.364 ± 0.106		[196]
VIPERS PDR2	0.60	0.49 ± 0.12	0.31	[210]
VIPERS PDR2	0.86	0.46 ± 0.09		[210]
BOSS DR12 voids	0.57	0.501 ± 0.051	0.307	[211]
2MTF 6dFGSv	0.03	0.404 ± 0.0815	0.3121	[212]
SDSS-IV	0.72	0.454 ± 0.139	0.31	[213]

inverse covariance matrix and P is the parameter space. The posterior distribution [see Eq. (B1)] is sampled using the Markov Chain Monte Carlo (MCMC) simulator through a suitably modified version of the publicly available code `CosmoMC` [187,188]. The statistical convergence of the MCMC chains for each model is set to satisfy the Gelman and Rubin criterion [214], $R - 1 \lesssim 0.01$.

The correction for the Alcock-Paczyński effect is taken into account by the fiducial correction factor, $\mathcal{R}$ [117,118] given as

$$\mathcal{R}(z) = \frac{H(z)D_A(z)}{H^{\rm fid}(z)D_A^{\rm fid}(z)} \tag{A7}$$

where $H(z)$ is the Hubble parameter and $D_A(z)$ is the angular diameter distance of the interacting models and that of the fiducial cosmology are denoted with superscript "fid." The corrected vector, $V^i_{f\sigma_8}(z,P)$ is corrected as

$$V^i_{f\sigma_8}(z_i,P) \equiv f\sigma^{\rm obs}_{8,i} - \frac{f\sigma^{\rm th}_8(z_i,P)}{\mathcal{R}(z_i)}, \tag{A8}$$

where $f\sigma^{\rm obs}_{8,i}$ is the ith observed data point from Table VII, $f\sigma^{\rm th}_8(z_i,P)$ is the theoretical prediction at the same redshift z_i and P is the parameter vector given by Eq. (34). The corrected $\chi^2_{f\sigma_8}$ is then written as

$$\chi^2_{f\sigma_8} = V^i_{f\sigma_8}\mathbf{C}^{-1}_{ij,f\sigma_8}V^j_{f\sigma_8}, \tag{A9}$$

where $\mathbf{C}^{-1}_{ij,f\sigma_8}$ is the inverse of the covariance matrix, $\mathbf{C}_{ij,f\sigma_8}$ of the $f\sigma_8$ dataset given by

$$\mathbf{C}_{ij,f\sigma_8} = \begin{pmatrix} \sigma_1^2 & 0 & \cdots & 0 & \cdots & 0 \\ 0 & \sigma_2^2 & \cdots & 0 & \cdots & 0 \\ \vdots & \vdots & \vdots & \vdots & \vdots & 0 \\ 0 & 0 & \cdots & \mathbf{C}_{\rm WiggleZ} & \cdots & 0 \\ 0 & 0 & \cdots & 0 & \mathbf{C}_{\rm SDSS\text{-}IV} & 0 \\ 0 & 0 & \cdots & 0 & \cdots & \sigma_N^2 \end{pmatrix} \tag{A10}$$

where $N = 27$ corresponds to total number of data points in Table VII. Thus the covariance matrix, $\mathbf{C}_{ij,f\sigma_8}$ is a 27×27 matrix with Eqs. (A2) and (A3) at the positions of $\mathbf{C}_{\rm WiggleZ}$ and $\mathbf{C}_{\rm SDSS-IV}$ respectively and σ_i is the error

from Table VII. To use the RSD measurements, we added a new likelihood module to the publicly available CosmoMC package to calculate the corrected $\chi^2_{f\sigma_8}$. The results obtained by analysing the MCMC chains are explained in Sec. IV.

APPENDIX B: MODEL SELECTION

Bayesian evidence is the Bayesian tool to compare models and is the integration of the likelihood over the multidimensional parameter space. Hence, it is also referred to as marginal likelihood. Using Bayes theorem, the posterior probability distribution of a model, M with parameters Θ for the given particular dataset x is obtained as

$$p(\Theta|x,M) = \frac{p(x|\Theta,M)\pi(\Theta|M)}{p(x|M)}, \tag{B1}$$

where $p(x|\Theta,M)$ refers to the likelihood function, $\pi(\Theta|M)$ refers to the prior distribution and $p(x|M)$ refers to the Bayesian evidence. From Eq. (B1), the evidence follows as the integral over the unnormalized posterior distribution,

$$E \equiv p(x|M) = \int d\Theta p(x|\Theta,M)\pi(\Theta|M). \tag{B2}$$

To compare model M_i with the reference model M_j, the ratio of the evidences, called the Bayes factor is calculated.

TABLE VIII. Revised Jeffreys scale by Kass and Raftery to interpret the values of $\ln B_{ij}$ while comparing two models M_i and M_j.

$\ln B_{ij}$	Strength
$0 \le \ln B_{ij} < 1$	Weak
$1 \le \ln B_{ij} < 3$	Definite/Positive
$3 \le \ln B_{ij} < 5$	Strong
$\ln B_{ij} \ge 5$	Very strong

$$B_{ij} = \frac{p(x|M_i)}{p(x|M_j)}. \tag{B3}$$

The calculation of the multidimensional integral is undoubtedly computationally expensive. This problem is solved by the method developed by Heavens *et al.* [190,191], where the Bayesian evidence is estimated directly from the MCMC chains generated by CosmoMC. This method for evidence estimation is publicly available in the form of MCEvidence. The MCEvidence package provides with the logarithm of the Bayes factor, $\ln B_{ij}$. The value of $\ln B_{ij}$ is then used to assess if model M_i is preferred over model M_j and if so, what is the strength of preference, by using the revised Jeffreys scale (Table VIII) by Kass and Raftery [215]. Thus, if $\ln B_{ij} > 0$, model M_i is preferred over model M_j.

The results of model comparison from the Bayesian evidence are discussed in Sec. IV.

[1] A. G. Riess *et al.*, Astron. J. **116**, 1009 (1998).
[2] B. P. Schmidt *et al.*, Astrophys. J. **507**, 46 (1998).
[3] S. Perlmutter *et al.*, Astrophys. J. **517**, 565 (1999).
[4] D. M. Scolnic *et al.*, Astrophys. J. **859**, 101 (2018).
[5] D. J. Eisenstein, W. Hu, and M. Tegmark, Astrophys. J. **504**, L57 (1998).
[6] N. Aghanim *et al.* (Planck Collaboration), Astron. Astrophys. **641**, A6 (2020).
[7] M. Tanabashi *et al.*, Phys. Rev. D **98**, 030001 (2018).
[8] B. A. Reid *et al.*, Mon. Not. R. Astron. Soc. **404**, 60 (2010).
[9] S. Alam *et al.*, Mon. Not. R. Astron. Soc. **470**, 2617 (2017).
[10] T. M. C. Abbott *et al.*, Phys. Rev. D **98**, 043526 (2018).
[11] M. A. Troxel *et al.*, Phys. Rev. D **98**, 043528 (2018).
[12] T. M. C. Abbott *et al.*, Phys. Rev. Lett. **122**, 171301 (2019).
[13] S. Alam *et al.* (eBOSS Collaboration), Phys. Rev. D **103**, 083533 (2021).
[14] T. Padmanabhan, Phys. Rep. **380**, 235 (2003).
[15] E. J. Copeland, M. Sami, and S. Tsujikawa, Int. J. Mod. Phys. D **15**, 1753 (2006).
[16] L. Amendola, K. Kainulainen, V. Marra, and M. Quartin, Phys. Rev. Lett. **105**, 121302 (2010).
[17] D. Wands, J. De-Santiago, and Y. Wang, Classical Quantum Gravity **29**, 145017 (2012).
[18] A. Mehrabi, Phys. Rev. D **97**, 083522 (2018).
[19] M. Martinelli, N. B. Hogg, S. Peirone, M. Bruni, and D. Wands, Mon. Not. R. Astron. Soc. **488**, 3423 (2019).
[20] J. A. Frieman, C. T. Hill, A. Stebbins, and I. Waga, Phys. Rev. Lett. **75**, 2077 (1995).
[21] S. M. Carroll, Phys. Rev. Lett. **81**, 3067 (1998).
[22] R. R. Caldwell, R. Dave, and P. J. Steinhardt, Phys. Rev. Lett. **80**, 1582 (1998).
[23] V. Sahni and A. Starobinsky, Int. J. Mod. Phys. D **09**, 373 (2000).
[24] L. A. Ureña López and T. Matos, Phys. Rev. D **62**, 081302 (2000).
[25] S. M. Carroll, Living Rev. Relativity **4**, 1 (2001).

[26] P. J. E. Peebles and B. Ratra, Rev. Mod. Phys. **75**, 559 (2003).
[27] E. J. Copeland, M. R. Garousi, M. Sami, and S. Tsujikawa, Phys. Rev. D **71**, 043003 (2005).
[28] S. Sinha and N. Banerjee, J. Cosmol. Astropart. Phys. 04 (2021) 060.
[29] M. Li, Phys. Lett. B **603**, 1 (2004).
[30] D. Pavón and W. Zimdahl, AIP Conf. Proc. **841**, 356 (2006).
[31] W. Zimdahl and D. Pavón, Classical Quantum Gravity **24**, 5461 (2007).
[32] E. Elizalde, S. Nojiri, and S. D. Odintsov, Phys. Rev. D **70**, 043539 (2004).
[33] S. Nojiri and S. D. Odintsov, Gen. Relativ. Gravit. **38**, 1285 (2006).
[34] Z. Zhang, S. Li, X.-D. Li, X. Zhang, and M. Li, J. Cosmol. Astropart. Phys. 06 (2012) 009.
[35] L. P. Chimento and M. G. Richarte, Phys. Rev. D **85**, 127301 (2012).
[36] I. A. Akhlaghi, M. Malekjani, S. Basilakos, and H. Haghi, Mon. Not. R. Astron. Soc. **477**, 3659 (2018).
[37] A. Kamenshchik, U. Moschella, and V. Pasquier, Phys. Lett. B **511**, 265 (2001).
[38] N. Bilić, G. B. Tupper, and R. D. Viollier, Phys. Lett. B **535**, 17 (2002).
[39] M. C. Bento, O. Bertolami, and A. A. Sen, Phys. Rev. D **66**, 043507 (2002).
[40] T. Padmanabhan and T. R. Choudhury, Phys. Rev. D **66**, 081301 (2002).
[41] L. P. Chimento and M. G. Richarte, Phys. Rev. D **84**, 123507 (2011).
[42] Y. Wang, D. Wands, L. Xu, J. De-Santiago, and A. Hojjati, Phys. Rev. D **87**, 083503 (2013).
[43] R. Caldwell, Phys. Lett. B **545**, 23 (2002).
[44] S. M. Carroll, M. Hoffman, and M. Trodden, Phys. Rev. D **68**, 023509 (2003).
[45] B. Feng, X. Wang, and X. Zhang, Phys. Lett. B **607**, 35 (2005).
[46] Y.-F. Cai, H. Li, Y.-S. Piao, and X. Zhang, Phys. Lett. B **646**, 141 (2007).
[47] V. Sahni and A. Starobinsky, Int. J. Mod. Phys. D **15**, 2105 (2006).
[48] S. Tsujikawa, Classical Quantum Gravity **30**, 214003 (2013).
[49] M. Sami and R. Myrzakulov, Int. J. Mod. Phys. D **25**, 1630031 (2016).
[50] P. Brax, Rep. Prog. Phys. **81**, 016902 (2018).
[51] V. Sahni, Classical Quantum Gravity **19**, 3435 (2002).
[52] P. J. Steinhardt, Phil. Trans. A Math. Phys. Eng. Sci. **361**, 2497 (2003), https://www.jstor.org/stable/3559230.
[53] H. E. S. Velten, R. F. vom Marttens, and W. Zimdahl, Eur. Phys. J. C **74**, 3160 (2014).
[54] A. P. Billyard and A. A. Coley, Phys. Rev. D **61**, 083503 (2000).
[55] D. Pavón, S. Sen, and W. Zimdahl, J. Cosmol. Astropart. Phys. 05 (2004) 009.
[56] L. Amendola, M. Gasperini, and F. Piazza, J. Cosmol. Astropart. Phys. 09 (2004) 014.
[57] R. Curbelo, T. Gonzalez, G. Leon, and I. Quiros, Classical Quantum Gravity **23**, 1585 (2006).
[58] T. Gonzalez, G. Leon, and I. Quiros, Classical Quantum Gravity **23**, 3165 (2006).
[59] Z.-K. Guo, N. Ohta, and S. Tsujikawa, Phys. Rev. D **76**, 023508 (2007).
[60] G. Olivares, F. Atrio-Barandela, and D. Pavón, Phys. Rev. D **77**, 063513 (2008).
[61] C. G. Böhmer, G. Caldera-Cabral, R. Lazkoz, and R. Maartens, Phys. Rev. D **78**, 023505 (2008).
[62] C. Quercellini, M. Bruni, A. Balbi, and D. Pietrobon, Phys. Rev. D **78**, 063527 (2008).
[63] R. Bean, E. E. Flanagan, I. Laszlo, and M. Trodden, Phys. Rev. D **78**, 123514 (2008).
[64] M. Quartin, M. O. Calvão, S. E. Jorás, R. R. R. Reis, and I. Waga, J. Cosmol. Astropart. Phys. 05 (2008) 007.
[65] J.-H. He and B. Wang, J. Cosmol. Astropart. Phys. 08 (2008) 010.
[66] L. P. Chimento, Phys. Rev. D **81**, 043525 (2010).
[67] L. Amendola, V. Pettorino, C. Quercellini, and A. Vollmer, Phys. Rev. D **85**, 103008 (2012).
[68] V. Pettorino, L. Amendola, C. Baccigalupi, and C. Quercellini, Phys. Rev. D **86**, 103507 (2012).
[69] V. Salvatelli, N. Said, M. Bruni, A. Melchiorri, and D. Wands, Phys. Rev. Lett. **113**, 181301 (2014).
[70] W. Yang and L. Xu, Phys. Rev. D **89**, 083517 (2014).
[71] J. S. Wang and F. Y. Wang, Astron. Astrophys. **564**, A137 (2014).
[72] C. Caprini and N. Tamanini, J. Cosmol. Astropart. Phys. 10 (2016) 006.
[73] R. C. Nunes, S. Pan, and E. N. Saridakis, Phys. Rev. D **94**, 023508 (2016).
[74] A. Mukherjee and N. Banerjee, Classical Quantum Gravity **34**, 035016 (2017).
[75] W. Yang, S. Pan, and D. F. Mota, Phys. Rev. D **96**, 123508 (2017).
[76] S. Pan, A. Mukherjee, and N. Banerjee, Mon. Not. R. Astron. Soc. **477**, 1189 (2018).
[77] W. Yang, S. Pan, and J. D. Barrow, Phys. Rev. D **97**, 043529 (2018).
[78] W. Yang, S. Pan, E. D. Valentino, R. C. Nunes, S. Vagnozzi, and D. F. Mota, J. Cosmol. Astropart. Phys. 09 (2018) 019.
[79] L. Visinelli and S. Vagnozzi, Phys. Rev. D **99**, 063517 (2019).
[80] S. Vagnozzi, L. Visinelli, O. Mena, and D. F. Mota, Mon. Not. R. Astron. Soc. **493**, 1139 (2020).
[81] K. Bamba, S. Capozziello, S. Nojiri, and S. D. Odintsov, Astrophys. Space Sci. **342**, 155 (2012).
[82] Y. L. Bolotin, A. Kostenko, O. A. Lemets, and D. A. Yerokhin, Int. J. Mod. Phys. D **24**, 1530007 (2015).
[83] B. Wang, E. Abdalla, F. Atrio-Barandela, and D. Pavón, Rep. Prog. Phys. **79**, 096901 (2016).
[84] G. Caldera-Cabral, R. Maartens, and B. M. Schaefer, J. Cosmol. Astropart. Phys. 07 (2009) 027.
[85] L. P. Chimento and M. G. Richarte, Phys. Rev. D **86**, 103501 (2012).
[86] L. P. Chimento, M. G. Richarte, and I. E. S. García, Phys. Rev. D **88**, 087301 (2013).
[87] W. Yang, S. Pan, L. Xu, and D. F. Mota, Mon. Not. R. Astron. Soc. **482**, 1858 (2019).

[88] C. van de Bruck, J. Mifsud, and J. Morrice, Phys. Rev. D **95**, 043513 (2017).
[89] W. Yang, N. Banerjee, and S. Pan, Phys. Rev. D **95**, 123527 (2017).
[90] R. Rosenfeld, Phys. Rev. D **75**, 083509 (2007).
[91] W. Yang, N. Banerjee, A. Paliathanasis, and S. Pan, Phys. Dark Universe **26**, 100383 (2019).
[92] F. Beutler, C. Blake, M. Colless, D. H. Jones, L. Staveley-Smith, L. Campbell, Q. Parker, W. Saunders, and F. Watson, Mon. Not. R. Astron. Soc. **416**, 3017 (2011).
[93] A. J. Ross, L. Samushia, C. Howlett, W. J. Percival, A. Burden, and M. Manera, Mon. Not. R. Astron. Soc. **449**, 835 (2015).
[94] N. Kaiser, Mon. Not. R. Astron. Soc. **227**, 1 (1987).
[95] P. A. R. Ade, N. Aghanim *et al.* (Planck Collaboration), Astron. Astrophys. **571**, A20 (2014).
[96] M. Kilbinger *et al.*, Mon. Not. R. Astron. Soc. **430**, 2200 (2013).
[97] C. Heymans *et al.*, Mon. Not. R. Astron. Soc. **432**, 2433 (2013).
[98] K. K. Schaffer *et al.*, Astrophys. J. **743**, 90 (2011).
[99] A. van Engelen *et al.*, Astrophys. J. **756**, 142 (2012).
[100] A. Pourtsidou and T. Tram, Phys. Rev. D **94**, 043518 (2016).
[101] C. van de Bruck and J. Mifsud, Phys. Rev. D **97**, 023506 (2018).
[102] S. Mohanty, S. Anand, P. Chaubal, A. Mazumdar, and P. Parashari, J. Astrophys. Astron. **39**, 46 (2018).
[103] R. An, C. Feng, and B. Wang, J. Cosmol. Astropart. Phys. 02 (2018) 038.
[104] G. Lambiase, S. Mohanty, A. Narang, and P. Parashari, Eur. Phys. J. C **79**, 141 (2019).
[105] E. Ó Colgáin and H. Yavartanoo, Phys. Lett. B **797**, 134907 (2019).
[106] A. Banerjee, H. Cai, L. Heisenberg, E. O. Colgáin, M. M. Sheikh-Jabbari, and T. Yang, Phys. Rev. D **103**, L081305 (2021).
[107] A. Gómez-Valent and J. Solà, Europhys. Lett. **120**, 39001 (2017).
[108] Z. Sakr, S. Ilić, A. Blanchard, J. Bittar, and W. Farah, Astron. Astrophys. **620**, A78 (2018).
[109] L. Kazantzidis and L. Perivolaropoulos, Phys. Rev. D **97**, 103503 (2018).
[110] A. Gómez-Valent and J. S. Peracaula, Mon. Not. R. Astron. Soc. **478**, 126 (2018).
[111] J. Ooba, B. Ratra, and N. Sugiyama, Astrophys. Space Sci. **364**, 176 (2019).
[112] C.-G. Park and B. Ratra, Phys. Rev. D **101**, 083508 (2020).
[113] Y. Wang, D. Wands, G.-B. Zhao, and L. Xu, Phys. Rev. D **90**, 023502 (2014).
[114] W. Yang and L. Xu, Phys. Rev. D **90**, 083532 (2014).
[115] A. A. Costa, X.-D. Xu, B. Wang, and E. Abdalla, J. Cosmol. Astropart. Phys. 01 (2017) 028.
[116] S. Nesseris, G. Pantazis, and L. Perivolaropoulos, Phys. Rev. D **96**, 023542 (2017).
[117] B. Sagredo, S. Nesseris, and D. Sapone, Phys. Rev. D **98**, 083543 (2018).
[118] F. Skara and L. Perivolaropoulos, Phys. Rev. D **101**, 063521 (2020).
[119] H. A. Borges and D. Wands, Phys. Rev. D **101**, 103519 (2020).
[120] A. G. Riess, L. Macri, S. Casertano, H. Lampeitl, H. C. Ferguson, A. V. Filippenko, S. W. Jha, W. Li, and R. Chornock, Astrophys. J. **730**, 119 (2011).
[121] A. G. Riess, S. Casertano, W. Yuan, L. Macri, B. Bucciarelli, M. G. Lattanzi, J. W. MacKenty, J. B. Bowers, W. Zheng, A. V. Filippenko, C. Huang, and R. I. Anderson, Astrophys. J. **861**, 126 (2018).
[122] A. G. Riess, S. Casertano, W. Yuan, L. M. Macri, and D. Scolnic, Astrophys. J. **876**, 85 (2019).
[123] B. P. Abbott (T. L. S. Collaboration, and T. V. Collaboration), Nature (London) **551**, 85 (2017).
[124] S. Birrer, T. Treu, C. E. Rusu, V. Bonvin, C. D. Fassnacht, J. H. H. Chan, A. Agnello, A. J. Shajib, G. C.-F. Chen, M. Auger, F. Courbin, S. Hilbert, D. Sluse, S. H. Suyu, K. C. Wong, P. Marshall, B. C. Lemaux, and G. Meylan, Mon. Not. R. Astron. Soc. **484**, 4726 (2019).
[125] N. Aghanim *et al.* (Planck Collaboration), Astron. Astrophys. **607**, A95 (2017).
[126] N. Aghanim *et al.* (Planck Collaboration), Astron. Astrophys. **641**, A5 (2020).
[127] D. O. Jones *et al.*, Astrophys. J. **867**, 108 (2018).
[128] M. Rigault *et al.*, Astron. Astrophys. **644**, A176 (2020).
[129] T. Clifton, P. G. Ferreira, A. Padilla, and C. Skordis, Phys. Rep. **513**, 1 (2012).
[130] E. Di Valentino, A. Melchiorri, and J. Silk, Phys. Lett. B **761**, 242 (2016).
[131] J. L. Bernal, L. Verde, and A. G. Riess, J. Cosmol. Astropart. Phys. 10 (2016) 019.
[132] E. Di Valentino, A. Melchiorri, and J. Silk, Phys. Rev. D **93**, 023513 (2016).
[133] J. M. Ezquiaga and M. Zumalacárregui, Phys. Rev. Lett. **119**, 251304 (2017).
[134] U. Alam, S. Bag, and V. Sahni, Phys. Rev. D **95**, 023524 (2017).
[135] E. Di Valentino, A. Melchiorri, E. V. Linder, and J. Silk, Phys. Rev. D **96**, 023523 (2017).
[136] E. Di Valentino, A. Melchiorri, and O. Mena, Phys. Rev. D **96**, 043503 (2017).
[137] N. Frusciante and L. Perenon, Phys. Rep. **857**, 1 (2020).
[138] N. Jackson, Living Rev. Relativity **10**, 4 (2007).
[139] L. Verde, T. Treu, and A. G. Riess, Nat. Astron. **3**, 891 (2019).
[140] J. Alcaniz, H. Borges, S. Carneiro, J. Fabris, C. Pigozzo, and W. Zimdahl, Phys. Lett. B **716**, 165 (2012).
[141] H. Velten, H. A. Borges, S. Carneiro, R. Fazolo, and S. Gomes, Mon. Not. R. Astron. Soc. **452**, 2220 (2015).
[142] R. vom Marttens, L. Casarini, W. Zimdahl, W. Hipólito-Ricaldi, and D. Mota, Phys. Dark Universe **15**, 114 (2017).
[143] S. Kumar and R. C. Nunes, Phys. Rev. D **96**, 103511 (2017).
[144] S. Kumar, R. C. Nunes, and S. K. Yadav, Eur. Phys. J. C **79**, 576 (2019).
[145] N. B. Hogg, M. Bruni, R. Crittenden, M. Martinelli, and S. Peirone, Phys. Dark Universe **29**, 100583 (2020).
[146] E. Di Valentino, A. Melchiorri, O. Mena, and S. Vagnozzi, Phys. Dark Universe **30**, 100666 (2020).
[147] R. A. Battye and A. Moss, Phys. Rev. Lett. **112**, 051303 (2014).

[148] E. Di Valentino, A. Melchiorri, and J. Silk, Phys. Rev. D **92**, 121302 (2015).
[149] E. Di Valentino and S. Bridle, Symmetry **10**, 585 (2018).
[150] K. L. Pandey, T. Karwal, and S. Das, J. Cosmol. Astropart. Phys. 07 (2020) 026.
[151] S. Vagnozzi, Phys. Rev. D **102**, 023518 (2020).
[152] E. Di Valentino, A. Melchiorri, O. Mena, and S. Vagnozzi, Phys. Rev. D **101**, 063502 (2020).
[153] W Yang, E. Di Valentino, S. Pan, Y. Wu, and J. Lu, Mon. Not. R. Astron. Soc. **501**, 5845 (2021).
[154] W. Yang, E. Di Valentino, S. Pan, S. Basilakos, and A. Paliathanasis, Phys. Rev. D **102**, 063503 (2020).
[155] T. Clemson, K. Koyama, G.-B. Zhao, R. Maartens, and J. Väliviita, Phys. Rev. D **85**, 043007 (2012).
[156] A. A. Costa, X.-D. Xu, B. Wang, E. G. M. Ferreira, and E. Abdalla, Phys. Rev. D **89**, 103531 (2014).
[157] M. Chevallier and D. Polarski, Int. J. Mod. Phys. D **10**, 213 (2001).
[158] E. V. Linder, Phys. Rev. Lett. **90**, 091301 (2003).
[159] D. Pavón and B. Wang, Gen. Relativ. Gravit. **41**, 1 (2009).
[160] J. Väliviita, E. Majerotto, and R. Maartens, J. Cosmol. Astropart. Phys. 07 (2008) 020.
[161] J.-H. He, B. Wang, and E. Abdalla, Phys. Lett. B **671**, 139 (2009).
[162] E. Majerotto, J. Väliviita, and R. Maartens, Mon. Not. R. Astron. Soc. **402**, 2344 (2010).
[163] M. Gavela, D. Hernández, L. L. Honorez, O. Mena, and S. Rigolin, J. Cosmol. Astropart. Phys. 07 (2009) 034.
[164] B. M. Jackson, A. Taylor, and A. Berera, Phys. Rev. D **79**, 043526 (2009).
[165] G. Caldera-Cabral, R. Maartens, and L. A. Ureña López, Phys. Rev. D **79**, 063518 (2009).
[166] S. Chongchitnan, Phys. Rev. D **79**, 043522 (2009).
[167] J.-Q. Xia, Phys. Rev. D **80**, 103514 (2009).
[168] M. Gavela, L. L. Honorez, O. Mena, and S. Rigolin, J. Cosmol. Astropart. Phys. 11 (2010) 044.
[169] A. Mehrabi, S. Basilakos, and F. Pace, Mon. Not. R. Astron. Soc. **452**, 2930 (2015).
[170] H. Kodama and M. Sasaki, Prog. Theor. Phys. Suppl. **78**, 1 (1984).
[171] V. Mukhanov, H. Feldman, and R. Brandenberger, Phys. Rep. **215**, 203 (1992).
[172] C.-P. Ma and E. Bertschinger, Astrophys. J. **455**, 7 (1995).
[173] D. Wands, K. A. Malik, D. H. Lyth, and A. R. Liddle, Phys. Rev. D **62**, 043527 (2000).
[174] K. A. Malik, D. Wands, and C. Ungarelli, Phys. Rev. D **67**, 063516 (2003).
[175] K. A. Malik and D. Wands, J. Cosmol. Astropart. Phys. 02 (2005) 007.
[176] K. A. Malik and D. Wands, Phys. Rep. **475**, 1 (2009).
[177] A. Lewis, A. Challinor, and A. Lasenby, Astrophys. J. **538**, 473 (2000).
[178] J. De-Santiago, D. Wands, and Y. Wang, in *6th International Meeting on Gravitation and Cosmology* (Springer, Switzerland, 2012).
[179] W. Hu, Astrophys. J. **506**, 485 (1998).
[180] R. Bean and O. Doré, Phys. Rev. D **69**, 083503 (2004).
[181] C. Gordon and W. Hu, Phys. Rev. D **70**, 083003 (2004).
[182] N. Afshordi, M. Zaldarriaga, and K. Kohri, Phys. Rev. D **72**, 065024 (2005).
[183] W. Hu and N. Sugiyama, Astrophys. J. **444**, 489 (1995).
[184] U. Seljak and M. Zaldarriaga, Astrophys. J. **469**, 437 (1996).
[185] S. Dodelson, *Modern Cosmology* (Academic Press, Amsterdam, 2003).
[186] W. J. Percival and M. White, Mon. Not. R. Astron. Soc. **393**, 297 (2009).
[187] A. Lewis, Phys. Rev. D **87**, 103529 (2013).
[188] A. Lewis and S. Bridle, Phys. Rev. D **66**, 103511 (2002).
[189] Ì. Zubeldia and A. Challinor, Mon. Not. R. Astron. Soc. **489**, 401 (2019).
[190] A. Heavens, Y. Fantaye, E. Sellentin, H. Eggers, Z. Hosenie, S. Kroon, and A. Mootoovaloo, Phys. Rev. Lett. **119**, 101301 (2017).
[191] A. Heavens, Y. Fantaye, A. Mootoovaloo, H. Eggers, Z. Hosenie, S. Kroon, and E. Sellentin, arXiv:1704.03472.
[192] D. J. Eisenstein *et al.*, Astrophys. J. **633**, 560 (2005).
[193] C. Alcock and B. Paczyński, Nature (London) **281**, 358 (1979).
[194] E. Macaulay, I. K. Wehus, and H. K. Eriksen, Phys. Rev. Lett. **111**, 161301 (2013).
[195] C. Blake *et al.*, Mon. Not. R. Astron. Soc. **425**, 405 (2012).
[196] G.-B. Zhao *et al.*, Mon. Not. R. Astron. Soc. **482**, 3497 (2019).
[197] D. Huterer, D. L. Shafer, D. M. Scolnic, and F. Schmidt, J. Cosmol. Astropart. Phys. 05 (2017) 015.
[198] S. J. Turnbull, M. J. Hudson, H. A. Feldman, M. Hicken, R. P. Kirshner, and R. Watkins, Mon. Not. R. Astron. Soc. **420**, 447 (2012).
[199] M. J. Hudson and S. J. Turnbull, Astrophys. J. Lett. **751**, L30 (2012).
[200] M. Davis, A. Nusser, K. L. Masters, C. Springob, J. P. Huchra, and G. Lemson, Mon. Not. R. Astron. Soc. **413**, 2906 (2011).
[201] M. Feix, A. Nusser, and E. Branchini, Phys. Rev. Lett. **115**, 011301 (2015).
[202] C. Howlett, A. J. Ross, L. Samushia, W. J. Percival, and M. Manera, Mon. Not. R. Astron. Soc. **449**, 848 (2015).
[203] Y.-S. Song and W. J. Percival, J. Cosmol. Astropart. Phys. 10 (2009) 004.
[204] C. Blake, I. K. Baldry, J. Bland-Hawthorn, L. Christodoulou, M. Colless, C. Conselice, S. P. Driver, A. M. Hopkins, J. Liske, J. Loveday, P. Norberg, J. A. Peacock, G. B. Poole, and A. S. G. Robotham, Mon. Not. R. Astron. Soc. **436**, 3089 (2013).
[205] L. Samushia, W. J. Percival, and A. Raccanelli, Mon. Not. R. Astron. Soc. **420**, 2102 (2012).
[206] A. G. Sánchez *et al.*, Mon. Not. R. Astron. Soc. **440**, 2692 (2014).
[207] C.-H. Chuang *et al.*, Mon. Not. R. Astron. Soc. **461**, 3781 (2016).
[208] A. Pezzotta *et al.*, Astron. Astrophys. **604**, A33 (2017).
[209] T. Okumura *et al.*, Publ. Astron. Soc. Jpn. **68**, 38 (2016).
[210] F. G. Mohammad *et al.*, Astron. Astrophys. **619**, A17 (2018).

[211] S. Nadathur, P. M. Carter, W. J. Percival, H. A. Winther, and J. E. Bautista, Phys. Rev. D **100**, 023504 (2019).
[212] F. Qin, C. Howlett, and L. Staveley-Smith, Mon. Not. R. Astron. Soc. **487**, 5235 (2019).
[213] M. Icaza-Lizaola *et al.*, Mon. Not. R. Astron. Soc. **492**, 4189 (2020).
[214] A. Gelman and D. Rubin, Stat. Sci. **7**, 457 (1992).
[215] R. E. Kass and A. E. Raftery, J. Am. Stat. Assoc. **90**, 773 (1995).